INVESTIGATION ON THE PRESENCE OF DETACHMENTS IN AZULEJOS BY MEANS OF NON DESTRUCTIVE ACOUSTIC MAPPING

DETECÇÃO REMOTA DE DESTACAMENTOS EM AZULEJOS ATRAVÉS DE MAPAS ACÚSTICOS

INVESTIGATION ON THE PRESENCE OF DETACHMENTS OF GLAZED CERAMIC TILE PANELS BY MEANS OF NON DESTRUCTIVE ACOUSTIC MAPPING

SYNOPSIS

This Report includes the theoretical background and the results of an assessment of the ACoustic Energy Absorption Device (ACEADD) as a means to reveal the presence of hidden decay in azulejo panels, namely detachments from the supporting wall and glaze delaminations. The project results from a cooperation between the Institute of Acoustics and Sensor - O. M. Corbino of the Italian National Research Council (CNR_IDASC), which developed the device and successfully tested it on partially detached frescos, and Laboratório Nacional de Engenharia Civil which is engaged in a planned effort to develop means of diagnose and intervention for the conservation of azulejo tiles and panels.

RESUMO

O relatório inclui os princípios teóricos e os resultados da avaliação do ACoustic Energy Absorption Device (ACEADD) como instrumento para revelar destacamentos ocultos e delaminações do vidrado em painéis de azulejos. O estudo resultou de uma colaboração entre o Institute of Acoustics and Sensor - O. M. Corbino do National Research Council (CNR_IDASC) italiano, que desenvolveu o equipamento e o experimentou com sucesso em frescos parcialmente destacados, e o Laboratório Nacional de Engenharia Civil que tem em curso projectos de investigação tendentes ao diagnóstico e intervenção em painéis azulejares, com vista à sua conservação.

**INVESTIGATION ON THE PRESENCE OF DETACHMENTS IN AZULEJOS
BY MEANS OF NON-DESTRUCTIVE ACOUSTIC MAPPING**

PAGE INDEX

INVESTIGATION ON THE PRESENCE OF DETACHMENTS IN AZULEJOS
BY MEANS OF NON-DESTRUCTIVE ACOUSTIC MAPPING

FIGURE INDEX

INVESTIGATION ON THE PRESENCE OF DETACHMENTS IN AZULEJOS

BY MEANS OF NON DESTRUCTIVE ACOUSTIC MAPPING

"The cultural heritage may be defined as the entire corpus of material signs - either artistic or symbolic - handed on by the past to each culture and, therefore, to the whole of humankind. As a constituent part of the affirmation and enrichment of cultural identities, as a legacy belonging to all humankind, the cultural heritage gives each particular place its recognizable features and is the storehouse of human experience. The preservation and the presentation of the cultural heritage are therefore a corner-stone of any cultural policy"

UNESCO Draft Medium Term Plan 1990-1995; UNESCO, 25 C/4, 1989, p.57

1 - INTRODUCTION

Conservation science plays a strategic role in cultural heritage policy for those countries that consider the preservation of the richness and peculiarity of their own culture as fundamental. Advancements in methodological procedures and technology for the conservation and restoration must be assessed within this frame and thus considered as a leading branch of science. New technologies for diagnostics are particularly important, not only as an aid to conservation and restoration but also as a potential tool for preventive conservation, allowing problems to be anticipated and challenges to be met before decay is apparent or has even started to affect the assets that must be preserved. This is especially true for those countries that are bestowed with an extraordinarily rich patrimony, or in which this legacy has a distinctive national characteristic. Additionally, a cultural heritage-driven development in both science and technology will favour innovative insights in other fields, due to the challenging, almost extreme, measuring conditions which are often found.

Since the last decades of the twentieth century, innovative technologies have increasingly been applied in the cultural heritage domain, leading to ever increasing requirements in the reliability and standardization by the professionals in this field. This is especially true in diagnostic and conservation activities. Indeed, during this period there has been a growing sensibility in the international community towards the implementation of common protocols and the adoption of standards. This has lead to the creation, in 2004, of the European Committee for Standardization Technical Committee CEN/TC 346 - Conservation of Cultural Property composed by thirty participant nations. Currently presidency and secretariat are assigned to UNI, the Italian organism for standardization, which initially proposed the creation of the committee itself. Five groups constitute the committee whose activity is focused on the standardization of: terms and definitions; methods and analysis; characterization of materials; conservation planning; conservation and restoration practices; safeguard of movable and unmovable heritage. At present no ISO technical committee exists, nor has any ISO standard been implemented in the field of cultural heritage but the situation will eventually change and all research of a pre-normative nature may contribute to whatever documents will be produced in the future.

Non Destructive Testing (NDT) methods are widely adopted in many fields for diagnostics and, as the objects under study remain intact, are particularly suited for cultural heritage applications. These methods are commonly used to determine materials properties, evaluate object integrity or to certify the quality of a product. A NDT method does not alter the integrity of the object under investigation, nor does it cause permanent modification or damage to the object; in general a NDT does not impair the usefulness of the object. Evidently any diagnostic method must be based on some type of interaction with the object in order to obtain information regarding it; however, a non destructive tool shall satisfy requirements regarding sampling procedures, measurement conditions, device calibration and sensitivity, experimental result reliability, and operator qualification.

In many types of investigations, a synergic set of NDT methods is required in order to reliably establish conclusive diagnostics. In the validation procedure implementing a specific method the comparative analysis with other techniques is fundamental, although in practice this is not always easily done.

Furthermore, in most cases the results from NDT are relevant indications for acceptance and rejection criteria. For instance, in cultural heritage diagnostics the results of a non destructive inspection shall include the indication of whether the conservation state of the object under study is critical for its integrity or not, and whether the degree of deterioration requires specific actions or not. Thus the results should be able to help decision makers in the management of cultural heritage.

The main NDT methodological areas concern Acoustic Emission (AE), Ultrasonic Testing (UT), Infrared Testing (IRT), Electromagnetic Testing (ET), Magnetic Testing (MT), Radiographic Testing (RT), Optical Testing (OT) and so on. Acoustic techniques play an important role in many applications, and some are useful tools in cultural heritage applications. In the present work an acoustic method is presented as a diagnostic tool for the assessment of the conservation state of glazed ceramic tile panels. The method and the relative device, the ACoustic Energy Absorption Device (ACEADD), were developed at the Institute of Acoustics and Sensor - O. M. Corbino of the Italian National Research Council (CNR_IDASC). The method is able to reveal the presence of hidden detachments in typical multilayer structures of heritage interest, such as frescoes and mosaics. Cooperation between the Stone & Ceramics Division (NPC) of the Department of Materials of LNEC and the Italian CNR_IDASC led to the realization of an experimental investigation on glazed ceramic tile (azulejos) panels for the determination of degradation phenomena due to detachments from the supporting wall and glaze delaminations. In particular the study aimed at the validation of the acoustic method and the evaluation of its reliability with respect to the forms of deterioration affecting ceramic tiles.

In the following sections different topics are presented regarding the most urgent problems in ceramic tile conservation. Technical details of the measuring technique and procedure are discussed, although a comprehensive understanding of acoustic diagnostics for cultural heritage is beyond the scope of the present work. For this purpose a list of the major works to be found in literature is indicated in the Reference section for further deepening of the arguments. Section 2 presents the context in which the cooperation between LNEC and CNR is framed, highlighting the competences and the interests of the

two parts in the field of cultural heritage. Section 3 examines the relevance of the Portuguese azulejo heritage and deals with the major deterioration phenomena affecting ceramic tiles. Section 4 provides the theoretical bases to understand the ACEADD diagnostic method and the characteristics of the investigated systems from the acoustical point of view, while the principles of the specific acoustic diagnostic method are described in Section 5. Section 6 shows the selected locations where in situ measurements were carried out, at the National Tile Museum (Museu Nacional do Azulejo, MNAz) in Lisbon. Finally, Section 7 outlines the ACEADD measuring procedure, adopted for the present investigation, while the experimental results and different kinds of data analysis are presented in Section 8. Specific aspects regarding tile detachments, glaze delaminations and the repeatability of the method are taken into account in separate subsections. Final remarks can be found in the Conclusions, while a Glossary is provided helping the comprehension of different topics. Two annexes give details related to the evaluation of resonant frequencies and to the repeatability tests.

There can be no doubt that cultural heritage ranks among those particular contexts where the need for interdisciplinarity is more evident. The research activity must be oriented towards the development of reliable methods and sustainable solutions guided by the requirements of the professionals devoted to its preservation and management. Methodological advancements must be inspired by the principles of scientific metrology, in order to guarantee the quality of the diagnostic methods. Cultural heritage itself may be the crucible where all the expertises from different disciplines convene and mix up, with mutual enrichment. Thus, it becomes, not only the final receiver of the benefits of research, but also the background, the subject and the purpose of the transformation of conservation policy into action. In this way the cultural heritage becomes a very particular laboratory for a systematic and synergic approach to conservation science, aiming at a realistic cultural heritage-driven scientific and technological development based on sound metrological data.

2 - EXECUTIVE SUMMARY

The Institute of Acoustics and Sensor "O. M. Corbino" of the Italian National Research Council (CNR) in Italy developed a method and a new acoustic equipment to detect the existence of cavities within walls- the ACoustic Energy Absorption Device (ACEADD). The equipment automatically scans a given area of wall by emitting an acoustic excitation and recording the reflected energy. Excited by an acoustic field, a cavity such as a detachment behaves as a selective acoustic absorber while a rigid wall reflects back practically all the incident energy, thus the method is able to discriminate damaged and undamaged portions of a surface. Furthermore, cavities resonate at a frequency that is related to their size. Thus, a determination of resonance frequencies allows a forecasting of the size of subsurface cavities. Once the extension of defects in the x-y wall plane and their width in the z-axis are obtained by means of acoustic mapping and frequency analysis, an advanced comprehension of the degree of deterioration of any wall, painted, paneled or otherwise finished, may be achieved.

The ACEADD device was successfully tested in Italy for the detection of hidden detachments in frescoes and the Institute of Acoustics and Sensor "O. M. Corbino" and Laboratório Nacional de Engenharia Civil, sharing their interest and activity in the development of tools for the diagnostic of decay in cultural heritage, established a cooperation that led to an experimental program aiming at the assessment of the potential of an acoustic diagnostic method for the non destructive inspection of glazed ceramic tile panels. The attention was focused on the determination of deterioration phenomena, such as detachment from the supporting wall or glaze delamination, in the early stages when no decay is yet visually evident. The overall aim is to provide a diagnostic means to support preventive interventions in order to avoid the fall of tiles and prevent glaze loss with its pictorial content. The present report describes the method employed in this investigation, providing insights into acoustic diagnostics theory and the discussion of the experimental results of *in situ* measurements, realized on tile panels at the Portuguese National Tile Museum (MNAz) in Lisbon.

The experimental program, realized at the MNAz includes the realization of:
− three maps for the assessment of tile detachments from the wall on two panels at the older 18th century church, closed to visitors and provisionally used to house part of the extensive reserves of the museum inventory;
− three maps for the assessment of glaze delaminations on panels at the top level of the cloister, whose walls are covered with low set panels obviously affected by moisture and depicting extensive loss of glaze, attributable to a manufacturing defect, probably shivering;

− repeatability tests on a restricted data set for the assessment of the reliability of the method and for a first evaluation of the uncertainty of measurement;

− comparative analysis with the subjective knocking inspection on a selected panel (this technique is called *martelletto* in Italian);

− integration of data with the visible inspection of the panels under study.

As concerns the assessment of tile detachments, the acoustic diagnostic method appears to give indication about the presence of resonant cavities although the comparison with the subjective knocking inspection on one panel does not give an apparent agreement between the results. The knocking technique provides a means to achieve detection in most cases, even if subjective, confirmed by a long tradition. On the other hand, the ACEADD method clearly measured resonances both in the low and high frequency bands. The discrepancies may be caused by the fact that the two methods, although both are based on the principles of acoustics, differ in the type of excitations and in the type of receivers. Indeed a mass that can be excited by an impact may not be excited by an acoustic wave. Moreover the human ear and the microphone are very different acoustical instruments with different sensitivity curves; thus what it is measured by a microphone, may not be perceived by human hearing.

For glaze delamination inspection, the acoustic method appears suitable even for the determination of thin cavities, just a few micrometers deep, since a number of high frequency resonances were clearly found in the maps. This is particularly important because in the case of delamination there is, at present, no simple concurring method able to scan large areas of wall with relative rapidity. But further investigation is required to assess the minimum size of detectable defects. Repeatability tests were realized on a restricted data set and returned important indication about the precision of the method. Finally the resonance frequency values extrapolated from the experimental data were in good agreement with the expected range of values given by the theoretical model.

3 - THE COLLABORATION BETWEEN LNEC AND CNR_IDASC

Through its composite scientific network, the Italian National Research Council (CNR) plays a relevant role in the domain of cultural heritage knowledge and conservation science in Italy. The Department of Cultural Heritage (DPC) and the Department of Cultural Identity (DIC) of CNR gather a number of Institutes and dedicated single groups having different expertises with the aim of creating fruitful synergies between philological, historical, archaeological, scientific and technological studies. The institutes are involved in research activities regarding both national and international projects, with a particular attention for the European Union programs and the partnerships oriented to the Mediterranean area. In particular the Institute of Acoustics and Sensor "O. M. Corbino" – CNR_IDASC in Rome has a long tradition in the development and application of acoustic methods in the cultural heritage field. Since its foundation, CNR_IDASC was involved in studies regarding the acoustic quality of antique theatres, the detection of vibration produced by sound sources placed close to works of art, the subsoil and underwater prospecting by means of echographic techniques to reveal archaeological remains. The specific competences are mainly oriented towards the development of innovative methods for acoustic diagnostics and monitoring, but service activity is also provided by the institute.

In the last decade, the group of Physical Techniques for Cultural Heritage, operating in the Institute, implemented a specific method and the relative device for the determination of detachments in frescoes, validating the method in laboratory tests on artificial models and by means of *in situ* measurements on real frescoes.

Laboratório Nacional de Engenharia Civil (LNEC) in Lisbon is a public research institute encompassing virtually all branches of civil engineering and related areas. LNEC carries out research, including planned research of a strategic nature, developed on the basis of research lines considered as essential due to their interest in the European and National contexts. LNEC also carries out consultancy activities on a contract basis in structural engineering, geotechnics, hydraulics, environment, transportation, housing, building materials and components aiming at the quality and safety of works, at the protection and rehabilitation of the natural and built heritage and at the technological modernization and innovation.

The testing facilities at LNEC are available not only to its own staff but also to external researchers and research teams to develop projects within the scope of LNEC research programs. Such projects often include the participation of LNEC researchers as partners or coordinators. The present cooperation between CNR-IDASC and LNEC was integrated by a common interest for innovative testing technologies within one of LNEC's planned research projects aimed at identifying the forms of azulejo decay and develop preventive and remedial solutions.

In the present study, the shared interest in cultural heritage diagnostic tools led to an experimental program aiming at the assessment of the potential of the acoustic method for the inspection of glazed ceramic tiles. The attention was focused on the determination of deterioration phenomena in their early stage of formation, in order to prevent the fall of relevant parts of tiles. Additionally a comparative analysis was planned, starting with the comparison between the

ACEADD method and the *martelletto* knocking evaluation carried out by LNEC researchers. The results collected during the present work represent the first attempt of applying the ACEADD method to ceramic tile facades.

4 - IMPORTANCE OF THE PORTUGUESE AZULEJO HERITAGE

4.1- A historic overview

From its origin in the Middle East and flourishing in the Islamic world, glazed tiles spread to Spain and Portugal and subsequently to Italy, the Low Countries and most of Europe.

Introduced to Portugal from the factories of Seville, Manises and Paterna, azulejos (as glazed ceramic tiles are called in Portuguese) started being produced locally in the 16th century and developed as a preferred means of finishing architectural surfaces in the mid 17th century, when they became ubiquitous in palaces, churches, gardens and bourgeois houses. The prevailing cobalt blue painting over a white tin glaze, that is so readily associated with the baroque architecture of Portugal and Brazil, developed when that colour combination became fashionable under the influence of Ming porcelain brought to Europe by the Portuguese ships that made the China trade route).

Originally applied, as in other countries, as a decorative and protective finishing, the use of azulejos in Portugal took a new facies in the mid 17th century, when they started being closely integrated with architecture in a characteristic way by which the architecture of volumes cannot be understood without considering together the treatment of surfaces, see Fig.1a- Igreja de Jesus, Setúbal. By the early 18th century, at the peak of the blue period (called in Portugal - the cycle of the Masters) azulejo panels often represented memorable events or narrate a story sequentially and thus the walls "talked" graphically to their viewers, in a way that may be likened to the Renaissance frescoes in Italy and, in some cases, to graphic novels. At this time architects used azulejos with an unerring easiness that surprises us today and the glory of many heritage sites rests the more on its azulejos, as the exterior architecture is simple and unassuming (Figs.1b and 1c).

Later in the 18th century a new fad by which domains were populated by azulejo personae and animals spread and rooted. The aristocracy populated the stairs of their palaces with make-believe armed guards or servants inviting guests in (for example Fig.1d Paço dos Arcebispos, Santo Antão do Tojal). Children and animals observed from behind stair balusters (all painted in tile panels) while simulated street goers peeped to gardens from closed barred gates. The inextricability of Portuguese azulejos and architecture is nowhere more evident than in this trompe l'oeil world [2].

Eventually demand in Portugal grew so much that it could not be met locally, and tiles of specified design were actually imported to the country from Holland. Portugal, on the other side, never exported except to its own overseas possessions, mostly to Brazil, and so Portuguese azulejos remain a national feature. Thus, it is not surprising that azulejos are an important theme in Portugal and studies on their conservation are easily recognized as of national interest and relevance.

Figure 1: Integration of glazed tile ornamental coverings into architectural structures.

4.2 - Some relevant forms of decay

Azulejos are a durable architectural finishing, as proven by centuries-old panels that are still virtually undamaged. However, whole tiles or groups of tiles may be lost by detachment from the supporting walls. Detachments of this kind may be caused by a number of factors but, once a single tile comes loose, its expansions and vibration will tend to contribute to the detachment of adjoining tiles in a process that will, if not counteracted, result in the collapse of large areas. Thus, it is common to find detached areas in which tiles are held solely by their lateral adhesion to other tiles, often also detached from the wall in an alarming example of precarious equilibrium.

Azulejos also suffer from the inherent weakness of being a layered material in which the outer glazed layer can readily detach from the ceramic substratum when shear forces arise in the interface. Such is the case when the thermal expansion coefficients of both glaze and bisque are not finely attuned [1]. During the cooling phase after the last firing, whenever the bisque contracts more than the glaze, shear tensions may lead to local or widespread delamination (Figs.2a and 2b).
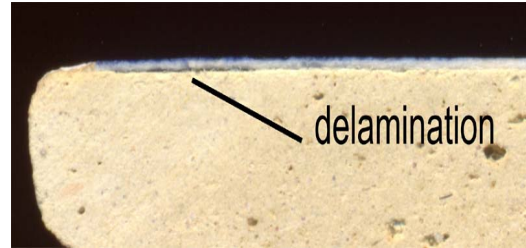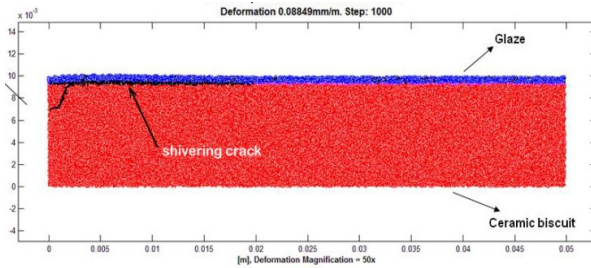
Figure 2: Delamination between clay bisque and glaze: (a) numerical model and (b) actual tile

This phenomenon, actually a manufacturing defect, is called "shivering" and often causes no alarming outside signals, rather it lays in waiting. When water moistens the biscuit, it will be able to penetrate in the open spaces under the glaze resulting from delamination, causing a characteristic bubble that breaks away leaving a lacuna wherefrom the process of detachment by salt crystallization later progresses. Cases are found nowadays where well over a third of the glazed surface has been lost [1] in a decay process that is in progression and will inevitably lead to the loss of whole panels of heritage value (Fig.3).

Figure 3: Generalized decay of an interior panel (Igreja de Jesus, Setúbal).

Detachments from the wall can often be detected by a process of knocking each tile with the fingers (similar to the Italian *martelletto* method). Delaminations caused by shivering, however, are not detectable and even when evident because of an ongoing loss of glaze, it is not easy to assess the remaining areas to check whether they are sound.

5 - ACOUSTIC PROPERTIES OF GLAZED CERAMIC TILES AND RELATED DETERIORATION PHENOMENA

Among Non Destructive Test (NDT) acoustic diagnostics is a useful tool to reveal the degree of deterioration in many objects belonging to cultural heritage. In particular the evaluation of acoustic energy absorption can be used to detect detachments and delaminations in *glazed ceramic tiles*, as well as in other artistic handiworks such as *plasters, frescoes* or *mosaics*. The response of such systems to an external acoustic excitation has to be analyzed, thus a scheme of the structure of the objects under investigation and a description of the relevant elements contributing to acoustically induced response of detachments is treated in the present section.

5.1- Multilayer Structure

Glazed ceramic tile panels can be considered as multilayer structures, mounted on an underlying supporting structure. When there is no evidence of deterioration and the adhesion between the layers is good, the acoustical properties of such systems are typical for highly reflecting materials. Assuming an acoustic plane wave normally incident on an infinitely rigid surface separating two different media, the action of the surface produces an additional field and the fraction of incident energy that is reflected by the surface, i.e. the intensity reflection coefficient, can be written as a function of the acoustic characteristic impedance Z_1 and Z_2 of the two media:

$$r = \frac{|p_r|^2}{|p_i|^2} = \frac{(Z_2 - Z_1)^2}{(Z_2 + Z_1)^2} \tag{1}$$

recalling that the incident and reflected acoustic intensity are proportional to the acoustic pressure respectively of the incident and reflected wave, p_i and p_r.

The characteristic acoustic impedance represents how the medium reacts to the perturbation of the acoustic field and is the product of the density ρ of the material and the acoustic wave velocity c. Different media present very different acoustic impedances. When the two impedances differ of several orders of magnitude total reflection occurs, and r approaches unity. This is the case in which the first medium is air and the second is a solid, such as typical building materials. The solid structure does not allow the wave to be transmitted inside the structure and the wave is totally back reflected. Table 1 shows the difference between the acoustically relevant properties of air compared to solid materials, for which the longitudinal wave velocity c_L is reported.

Medium	Density ρ kg m^{-3}	Sound velocity c_L m s^{-1}	Acoustic Impedance Z Pa s m^{-1}
Air (@20°C)	1.2	343	415
Clay	2.2E+3	3400	7.5E+6
Quartz	2.6E+3	5450	1.4E+7

Table 1: Properties of different media.

The fraction of incident energy that is not reflected back by the surface is the acoustic energy absorption coefficient α equal to (**1 - *r***) [3]. Therefore highly reflecting surfaces show very low values of absorption coefficient; for instance

many building materials show values of **α** less than 0.05 in the whole frequency range of interest in architectural acoustics, as reported in Table 2. Thus the amount of energy absorbed by a material is mainly determined by its characteristic acoustic impedance.

Materials	63Hz	125Hz	250Hz	500Hz	1kHz	2kHz	4kHz	8kHz
Rough Concrete	0.0200	0.0200	0.0300	0.0300	0.0300	0.0400	0.0700	0.0700
Brick, unglazed, painted	0.0100	0.0100	0.0100	0.0200	0.0200	0.0200	0.0300	0.0300
Marble or glazed tile	0.0100	0.0100	0.0100	0.0100	0.0100	0.0200	0.0200	0.0200
Plaster, gypsum, or lime, rough finish on lath	0.1400	0.1400	0.1000	0.0600	0.0500	0.0400	0.0300	0.0300
Acoustic plaster	0.1500	0.1500	0.2500	0.4000	0.5500	0.6000	0.6000	0.6000
Sand, 100 mm thickness	0.1500	0.1500	0.3500	0.4000	0.5000	0.5500	0.8000	0.8000
10 mm soft carpet on concrete	0.0900	0.0900	0.0800	0.2100	0.2600	0.2700	0.3700	0.3700

Table 2: Acoustic absorption coefficient by the *Reverberation Room Method (UNI EN ISO 354:2003)* of some typical building materials, given at 1/3 octave band frequencies [4, 5].

5.2- Detachments and delaminations

Particular environmental conditions as well as the quality of the glazing and its exposure may influence the status of conservation, as discussed in Section 4. Thus decay (detachments and/or delaminations) phenomena may occur with the creation of air cavities between layers.

The presence of detachments between two adjacent layers gives specific elastic properties to the structure, so that it can no more be depicted as an infinitely rigid system. The system indeed consists of a thin surface layer (for which the thickness is much less than the extension of the detached area), separated from the supporting structure (still infinitely rigid) by an air cavity, as shown in Fig.4.
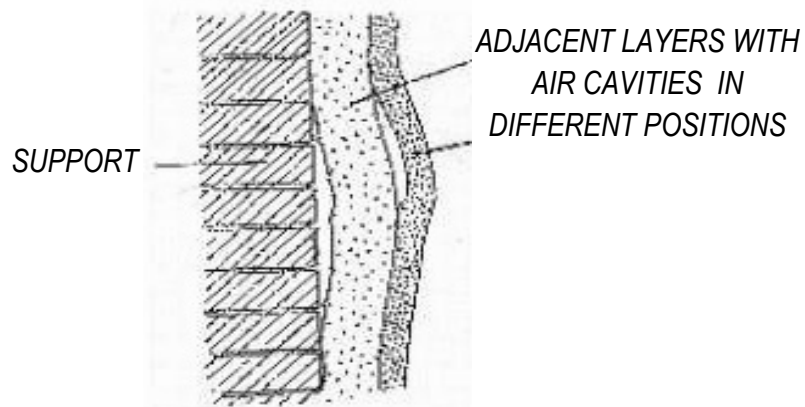
Figure 4: Examples of detachments in a multilayer structure.

Due to the action of a pressure field generated by an acoustic source the surface layer vibrates, thanks to the elasticity of the system layer-cavity, producing an additional pressure field. It radiates back a fraction of the incident acoustic energy, so that the overall acoustic field results from two components, one produced by the external source and the second generated by the vibrating surface. The theoretical model describing a vibrating surface allows us to evaluate relevant characteristics of the pressure field in the free half plane. Few important elements contribute to the acoustic behavior of detachments and delaminations:

- The vibrating surface model;
- The influence of boundaries;
- The effects of cavities;
- The forced vibration of surface and resonant behavior;
- Dissipative effects;
- The relation with acoustic energy absorption phenomena.

5.3- Theoretical model of a vibrating surface

To represent the uppermost detached layer, the model of a vibrating thin plate is considered, starting from the analysis of free vibrations. Bending (or flexural) waves may propagate on the surface, with the displacement transverse to the direction of propagation, thus causing a perturbation of an adjacent fluid. Assuming the surface extends in the xy plane, the fourth order bending wave equation of motion can be written as follows:

$$\nabla^2\left(\nabla^2\zeta\right)+\left[\frac{\rho\left(1-\varepsilon^2\right)}{E\kappa^2}\right]\frac{\partial^2\zeta}{\partial t^2}=0 \tag{2}$$

where ζ is the displacement along the z axis, ∇^2 is the two-dimensional Laplacian operator, ρ is the volume density, E is Young's modulus, ε is Poisson's ratio, and κ is the radius of gyration that is related to the shape of the system [3,6]. The equation takes into account the balance between the bending moment and the restoring force due to the plate stiffness.

The solution of Eq. 2 for periodic vibrations can be separated in two functions containing the dependence on the spatial and temporal coordinates respectively. The choice of a proper set of coordinates depends on surface shape, thus for a rectangular surface the Cartesian coordinates are taken, while for a circular surface the polar coordinates are preferred. Let us consider this last case (circular shape), for which the displacement is written as:

$$\zeta=\psi(r,\varphi)e^{i\omega t} \tag{3}$$

yielding the following solution for *(r,φ):*

$$\nabla^2\left(\nabla^2\psi\right)-K^4\psi=0, \quad K \text{ being the wave vector}: K^4=\left[\frac{\omega^2\rho\left(1-\varepsilon^2\right)}{E\kappa^2}\right] \tag{4}$$

The solutions of Eq. 4, assuming finite displacement at the centre of the surface, are of the following kind:

$$\psi_{m,n}(r,\varphi) = \cos(m\varphi)\left[AJ_n(Kr) + BI_n(Kr)\right] \qquad (5)$$

where $J_n(Kr)$ and $I_n(Kr)$ are respectively the n order Bessel and modified Bessel functions.

5.4 - Boundary conditions

The boundary conditions define the allowed values of K for free vibrations, and the assumption of an ideal model is required. Assuming the circular surface is rigidly clamped all around the circumference, at $r = a$, boundary conditions are:

$$\psi(a) = 0; \quad \left.\frac{\partial \psi}{\partial r}\right|_a = 0 \qquad (6)$$

yielding:

$$\begin{cases} AJ_n(Ka) + BI_n(Ka) = 0 \\ I_n(Ka)\left.\frac{dJ_n(Kr)}{dr}\right|_a - J_n(Ka)\left.\frac{dI_n(Kr)}{dr}\right|_a = 0 \end{cases} \qquad (7)$$

which are satisfied only at particular values of Ka:

$$K_{m,n}\, a = \pi\, \beta_{m,n} \quad \text{with:}$$

$\beta_{0,1} = 1.015$	$\beta_{0,2} = 2.007$	$\beta_{0,3} = 3.000$
$\beta_{1,1} = 1.468$	$\beta_{1,2} = 2.483$	$\beta_{1,3} = 3.490$
$\beta_{2,1} = 1.879$	$\beta_{2,2} = 2.992$	$\beta_{2,3} = 4.000$

(8)

The allowed set of bending wave vectors $K_{m,n}$ are related to the set of functions $\psi_{m,n}$ and to the set of frequencies $f_{m,n}$, the natural frequencies of the thin plate, obtained by substituting the allowed wave vector into Eq. 4 and solving with respect to ω. Therefore standing wave patterns on the surface are produced. Each mode of vibration is identified by the pair *(m, n)* where *m* denotes the number of radial nodal lines and *n* denotes the number of azimuthal nodal circles, presented schematically in Table 3.
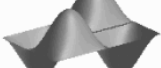
Bending wave vectors	Natural frequencies	
$K_{0,n} = \dfrac{3.20}{a}, \quad \dfrac{6.30}{a}, \quad \dfrac{9.44}{a}, \quad \dots$ $K_{1,n} = \dfrac{4.61}{a}, \quad \dfrac{7.80}{a}, \quad \dfrac{10.96}{a}, \quad \dots$ $K_{2,n} = \dfrac{5.90}{a}, \quad \dfrac{9.40}{a}, \quad \dfrac{12.57}{a}, \quad \dots$	$f_{0,1} = \dfrac{\omega_{m,n}}{2\pi} = \dfrac{K_{m,n}^2}{2\pi}\sqrt{\dfrac{E\kappa^2}{\rho(1-\varepsilon^2)}}$ $f_{0,1} = \dfrac{\omega_{0,1}}{2\pi} = \dfrac{10.24}{2\pi a^2}\sqrt{\dfrac{E\kappa^2}{\rho(1-\varepsilon^2)}}$ $f_{0,2} = \left(\dfrac{6.30}{3.20}\right)^2 f_{0,1} = 3.88 f_{0,1}$ $f_{0,3} = \left(\dfrac{9.44}{3.20}\right)^2 f_{0,1} = 8.70 f_{0,1}$ etc.	Mode (0,1) Mode (1,1) Mode (2,1) Mode (0,2) Mode (1,2) Mode (0,3)

Table 3: Allowed values of wave vector and related frequencies for a circular plate. The specific ratios between overtones and the fundamental frequency are also shown. The image on the right is teaching material of the Institute of Sound and Vibration Research *ISVR*, University of Southampton.

Similarly for a rectangular panel, $L_x \times L_y$ in size and clamped at its edge, standing wave patterns are produced. For the boundary conditions, L_x and L_y can only match an integer number of the allowed half wavelength:

$$K^2 = K_x^2 + K_y^2 \qquad K_{x,m} = \frac{2\pi}{\lambda_m} = m\frac{\pi}{L_x}; \quad K_{y,n} = \frac{2\pi}{\lambda_n} = n\frac{\pi}{L_y}; \quad m,n = 1,2,3,\dots \quad (9)$$

The natural modes of vibration of a rectangular panel are schematically reported in Table 4.

Bending wave vectors	Natural frequencies	
$K_{m,n} = \left[\left(\dfrac{m\pi}{L_x}\right)^2 + \left(\dfrac{n\pi}{L_y}\right)^2\right]^{1/2}$	$f_{m,n} = \dfrac{\omega_{m,n}}{2\pi} = \dfrac{K_{m,n}^2}{2\pi}\sqrt{\dfrac{E k^2}{\rho(1-\varepsilon^2)}}$ $f_{m,n} = \dfrac{\pi}{2}\sqrt{\dfrac{E\kappa^2}{\rho(1-\varepsilon^2)}}\left[\left(\dfrac{m}{L_x}\right)^2 + \left(\dfrac{n}{L_y}\right)^2\right]$	Mode (1,1) Mode (1,2) Mode (2,1) Mode (2,2)

Table 4: Allowed values of wave vector and related frequencies for a rectangular plate. The image on the right is teaching material of the Institute of Sound and Vibration Research *ISVR*, University of Southampton.

5.5 - The effect of cavities

Assuming that a vibrating surface is fixed to a rigid support with a closed space in between, the surface induces pressure changes inside the cavity. The volume of

air undergoes compression and rarefaction and the total effect on the volume depends on the average displacement of the vibrating surface:

$$dV = S\langle \zeta \rangle_S \tag{10}$$

where **S** is the surface area, assuming an equal extension of the cavity.

Since it is an adiabatic process, the following equation can be used to obtain the variation of pressure inside the enclosed volume:

$$PV^{\gamma} = P_0 V_0^{\gamma} \tag{11}$$

where γ is the ratio of specific heats (5/2 for diatomic gas such as air), and the index 0 denotes the steady state. Differentiating Eq. (11) **dP** is therefore obtained

$$dP = -\frac{\gamma P_0}{V_0} dV = -\frac{\gamma P_0}{V_0} S \langle \zeta \rangle_S \tag{12}$$

Writing Eq. (12) in terms of the variation of force **df** acting on the surface:

$$df = -\frac{\gamma P_0}{V_0} S^2 \langle \zeta \rangle_S = -\frac{c_0^2 \rho_0}{V_0} S^2 \langle \zeta \rangle_S , \tag{13}$$

with **ρ_0** the density of air and **c_0** the sound speed in air, it can be assessed that there is a further elastic force exerted on the surface by the volume of air inside the cavity.

Thus such an *air-spring* has a characteristic elasticity **k_{air}**:

$$k_{air} = \frac{c_0^2 \rho_0}{V_0} S^2 = \frac{c_0^2 \rho_0}{d} S \tag{14}$$

where **d** is the cavity thickness. Eq. (13) represents an additional term that has to be included in the bending wave equation, Eq. (2), representing the restoring force acting on the surface and it has to be compared to the restoring force due to the stiffness of the surface layer.

5.6 - Forced Vibration

Most acoustic diagnostic methods are based on the interaction of an acoustic field with the structure under investigation, thus undergoing forced vibrations. To study an elastic system, such as those described before, subject to an external perturbation, the following equation has to be solved:
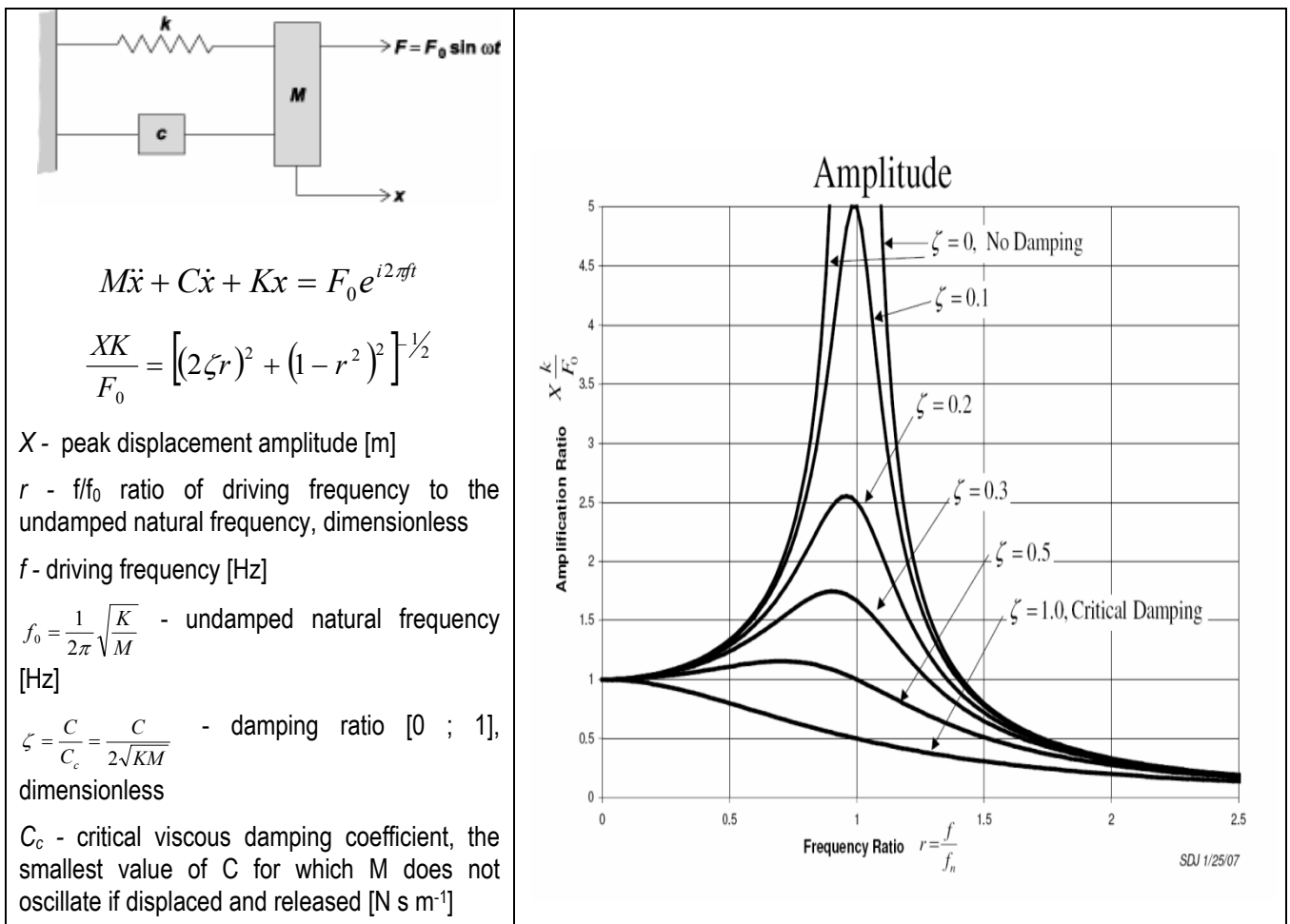
$$\left[\frac{E\kappa^2 St}{(1-\varepsilon^2)}\right] \nabla^2 (\nabla^2 \zeta) + M \frac{\partial^2 \zeta}{\partial t^2} + \frac{c_0^2 \rho_0}{d} S \langle \zeta \rangle_S = Fe^{i\omega t} \tag{15}$$

where **t** is the layer thickness and no additional damping mechanisms were considered.

If the perturbation contains specific frequencies, the consequent vibration of the system includes only those frequencies present in the perturbation. The relevant aspect is that when the perturbation frequency content approaches the natural frequencies of the system, resonant phenomena occur and the displacement amplitude tends to infinity.

The response of the system at resonance is unbounded unless part of the energy is dissipated, and real systems are characterized by damping mechanisms, that need to be taken into account. Damping may take place due to internal friction with transformation of energy into heat, or due to transmission of energy into contiguous structures (at the boundaries) and into contiguous fluids (radiation damping). In Fig. 5 the classical problem of forced and damped vibration of a mass-spring-damper system is summarized with amplification ratio curves (amplitude × rigidity / driving force) for different damping ratios are shown on the right.

$$M\ddot{x} + C\dot{x} + Kx = F_0 e^{i2\pi ft}$$

$$\frac{XK}{F_0} = \left[(2\zeta r)^2 + (1 - r^2)^2 \right]^{1/2}$$

X - peak displacement amplitude [m]

r - f/f_0 ratio of driving frequency to the undamped natural frequency, dimensionless

f - driving frequency [Hz]

$f_0 = \frac{1}{2\pi}\sqrt{\frac{K}{M}}$ - undamped natural frequency [Hz]

$\zeta = \frac{C}{C_c} = \frac{C}{2\sqrt{KM}}$ - damping ratio [0 ; 1], dimensionless

C_c - critical viscous damping coefficient, the smallest value of C for which M does not oscillate if displaced and released [N s m^{-1}]

Figure 5: The mass-spring-damper problem, for viscous damping, and amplification curves for different values of damping ratio [7].

Resonant response of the system (at $f = f_0$) is damping-controlled; as frequency decreases, the response is stiffness-controlled (at $f < f_0$) while it is mass-controlled as frequency increases (at $f > f_0$).

On the basis of these considerations, the theoretical model of an absorbing panel with a cavity of air between the panel and the supporting wall, can be used for both detachments and delaminations in order to evaluate expected resonance

frequencies. The properties of the system are equivalent of typical panel absorbers commonly used in buildings, the double-wall systems, whose function is to absorb low frequency energy by resonance in its fundamental bending mode. The problem is that of a double-wall resonance where the supporting wall is much more massive than the superficial layer. In this model the air cavity stiffness, rather than the panel stiffness determines the resonance frequency (Eq. 15), easily calculated representing the system by a harmonic oscillator model where the mass **M** is concentrated in the superficial layer and the spring rigidity is that of the air volume **k_{air}** [6, 7]:

$$f_0 = \frac{1}{2\pi}\sqrt{\frac{k_{air}}{M}} = \frac{c_0}{2\pi}\sqrt{\frac{\rho_0}{\rho_S d}} \tag{16}$$

where ρ_s is the panel surface density (i.e. the product of the volume density ρ times the surface layer thickness t). In this model the section of the cavity equals the area of the vibrating panel.

The values of the fundamental frequency for a variety of cases were evaluated on the basis of experimental data on azulejo samples analyzed at UFPA-Universidade Federal do Pará [8] and reported in Tab. 5. In particular sample P5 was taken as representative even if data shows a wide range in composition, porosity, density and thickness (the values are reported in Annex 2).

Material	Density	Layer thickness	Cavity depth	Panel + Air cavity
	ρ (kg/m3)	t (m)	d (m)	f0 (Hz)
Tile [P5]	1.75E+03	1.00E-02	0.001	4.69E+02
Glaze [P5]	7.25E+03	3.00E-04	0.0001	4.21E+03
Air	1.292			

Table 5: Estimated values of fundamental frequency for tile panel and glazed layer for a particular case, sample P5 analyzed at UFPA[8].

Resonance frequency values for tile panel and glaze panel (referred to P5 sample) were calculated for different depths of air cavity, shown in Tab. 6.

Cavity depth d (mm)	Tile f0 (Hz)	Cavity depth d (mm)	Glaze f0 (Hz)
9.00E-01	4.94E+02	1.00E-01	4.21E+03
8.00E-01	5.24E+02	9.00E-02	4.44E+03
7.00E-01	5.61E+02	8.00E-02	4.70E+03
6.00E-01	6.06E+02	7.00E-02	5.03E+03
5.00E-01	6.63E+02	6.00E-02	5.43E+03
4.00E-01	7.42E+02	5.00E-02	5.95E+03
3.00E-01	8.56E+02	4.00E-02	6.65E+03
2.00E-01	1.05E+03	3.00E-02	7.68E+03
1.00E-01	1.48E+03	2.00E-02	9.41E+03
5.00E-02	2.10E+03	1.00E-02	1.33E+04
1.00E-02	4.69E+03	5.00E-03	1.88E+04

Table 6: Fundamental frequency for tile panel (10mm thick) and glazed layer (0.3mm thick) for different depths of air cavity.

It can be easily noted that tile detachments with an enclosed volume of air behind of less than 1mm present resonance frequencies of less than 1 kHz, while delaminations of the glazed layer present resonance frequencies in the range 5 KHz up to the limit of the acoustical device (and human perception) around 20 kHz. Thus using the ideal model for panel-cavity systems, a driving frequency in the audible frequency band is suitable for the excitation of the system, in presence of both detachments and delaminations.

5.7 - Damping mechanisms

At any time a vibrating structure holds a certain amount of kinetic energy and of potential energy; the kinetic energy storage is associated with the mass while the potential energy storage is associated with the stiffness. Moreover all real systems dissipate some energy through different damping mechanisms, converting mechanical energy into thermal energy or transferring it to contiguous structures and fluids [7].

Employing the simple model of mass-spring-damper described in Fig. 5, the response of the system will be: $x(t)=X\ sin(\omega t+\Phi)$, while kinetic energy and potential energy assume the well known forms:

$$\begin{cases} E_{kin} = \dfrac{M}{2}\dot{x}^2 = \dfrac{M}{2}\omega^2 X^2 \cos^2(\omega t + \varphi) \\ E_{pot} = \dfrac{K}{2}x^2 = \dfrac{K}{2}X^2 \sin^2(\omega t + \varphi) \end{cases} \quad E_{tot} = E_{kin} + E_{pot} = \dfrac{M}{2}\omega^2 X^2 + \dfrac{K}{2}X^2 = 2E_{pot,\max} = KX^2 \atop @\,\omega = \omega_0 \quad (17)$$

Assuming viscous damping, the differential amount of energy dissipated is $C\dot{x}\,dx = C\dot{x}^2\,dt$ that, integrated over a whole cycle, gives the amount of energy:

$$D = CX^2\omega^2 \int_0^T \cos^2(\omega t + \varphi)dt \ . \tag{18}$$

The *loss factor* or *dissipation factor* η, characteristic of the damping mechanism, is written as follows

$$\eta = \frac{D/2\pi}{E_{pot,\max}} = \frac{C\omega}{K} = 2\zeta r \ , \tag{19}$$

whose value equals *2ζ* at resonance (*r = 1*), i.e. when the response is damping controlled. For viscous damping the loss factor is proportional to frequency, as shown in Eq. 19; but different damping mechanisms may superpose and their loss factors may show different frequency dependencies. Thus a *total loss factor* has to be considered, as sum of all the causes of energy dissipation. For this purpose the damping action of a composite structure, such as an absorbing panel, can be schematically depicted as a system of springs, each spring representing an energy storage mechanism with a specific loss factor. When the panel is deflected, the deflection is transferred to the springs, so that each one deflects x_i and stores an amount of energy $E_i = (k_i/2)\ (x_i)^2$. The energy dissipated

by the ith spring per cycle is therefore $D_i = 2\pi\eta_l E_i$ where η_i is the loss factor of ith spring [6]. The total loss factor can be defined as:

$$\eta_{tot} = \frac{\sum \eta_i E_i}{\sum E_i} = \frac{\sum \eta_i K_i x_i^2}{\sum K_i x_i^2} \,. \tag{20}$$

The determination of all damping components is not simple, so we shall restrict to the ideal case of a panel-cavity system focusing on the aspects relevant to absorption.

5.8 - Acoustic energy absorption coefficient

Let us consider the model of a surface layer, with a cavity adjoining a backing rigid wall. At mass-spring resonance the absorption is maximized due to the effects of different mechanisms. For the ideal model of detachment or delamination, the absorption is due to surface layer vibration, the presence of the cavity, the back wall and the contiguous structures and fluids, and the internal loss of the surface layer. The principal contribution was demonstrated to be ascribed to the energy absorption in the back cavity while the panel internal loss and radiation give minor contributions. Different approaches were used to determine theoretical curves for the absorption coefficient [9-11]. Assuming the structure under study is a multi-layer system for which can be defined a complex surface impedance Z, the normal incidence absorption coefficient is:

$$\alpha = \frac{4\rho_0 c_0 \,\mathrm{Re}(Z)}{\left(\mathrm{Re}(Z) + \rho_0 c_0\right)^2 + \left(\mathrm{Im}(Z)\right)^2} \tag{21}$$

The *Transfer Matrix* approach to modeling the sound propagation in a multi-layer system allow the determination of the surface impedance of such a system [11], that can be written as follows:

$$Z = m\omega_0\eta + i\left[\omega m - \rho_0 c_0 \cot(k_0 d)\right] \tag{22}$$

where in this case m denotes the mass per unit area of the panel. At mass-spring resonance the imaginary part is zero (giving the same result as Eq. 16) and the absorption coefficient becomes

$$\alpha(\omega_0) = \frac{4\rho_0 c_0 m\omega_0\eta}{\left(m\omega_0\eta + \rho_0 c_0\right)^2} \qquad\qquad \text{with} \quad Z = m\omega_0\eta \,. \tag{21}$$

The main feature of this kind of structures is the presence of a low frequency resonance in the absorption coefficient curve, as represented in Fig. 6 in comparison with other common absorber curves such as the Helmholtz resonator (cavity absorber) with a very sharp peak and dissipative absorber (porous material) with a typical broad high frequency absorption. When absorption curves are reported, a particular attention has to be paid to which kind of absorption coefficient is considered, *oblique incidence* or *normal incidence* absorption coefficient, or *diffuse field* absorption coefficient. The measuring procedures are different and differences in the absorption curves occur.
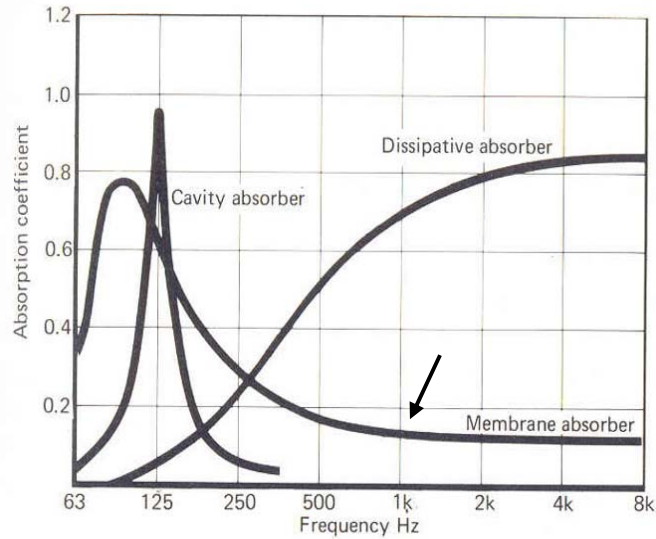
Figure 6: Characteristic sound absorption curves, showing the low frequency resonance for *membrane absorber*. *Cavity absorber* and *dissipative absorber* curves are also shown.

5.9 - Real cases

The determination of the absorption coefficient of a real system (tile-cavity-wall or glaze-cavity-body) is not a simple matter due to the heterogeneity of the structure, the variety of bonding conditions and constituent materials. All these characteristics influence the values of important parameters and the acoustic behavior of the system. The model adopted until now to represent a detached area of a tile panel, or its surface glazed layer, is a schematic view which takes advantage of the correspondence of these structures to *membrane absorbers*, commonly used for noise control in buildings. Actually a detachment or a delamination presents uneven shapes and boundary conditions far from the ideal case, furthermore the depth of air cavity may be very different and not uniform over the detachment extension. Differences in material composition and in the technique of realization may affect the properties of both the surface layer and the back wall. The great number of variables and the distance of a real system from the ideal model make any theoretical analysis very difficult, and more accurate models may be achieved by means of *Finite Elements Analysis*. Such an approach is beyond the purpose of the present work, whose aim is to demonstrate the usefulness of the measurement of the acoustic absorption coefficient as a proper indicator of the presence of tile detachments and glaze delaminations.

6 - THE ACOUSTIC DIAGNOSTIC METHOD AND DEVICE: ACEADD

The ACEADD device identifies anomalous acoustic behavior in absorption processes of decorative mural structures, through a non-contact 2D scan over the surface under investigation using a back reflection geometry. The method provides acoustic images of the surface, building 2D or 3D maps, where detached areas are discriminated from undamaged ones [12-14]. As described in the previous section, under acoustic field excitation, a detachment behaves as a selective acoustic absorber while a rigid wall reflects back all the incident energy.

The diagnostic device, shown in Fig.7, is composed of four basic units:

1- the _transceiver unit_ composed of a full range sound source S (_100 Hz : 20 kHz_) and a miniature omni-directional wide band microphone M, in coaxial configuration;
2- the _transducers circuitry unit_ for signal generation and recording;
3- _remotely controlled scan unit_;
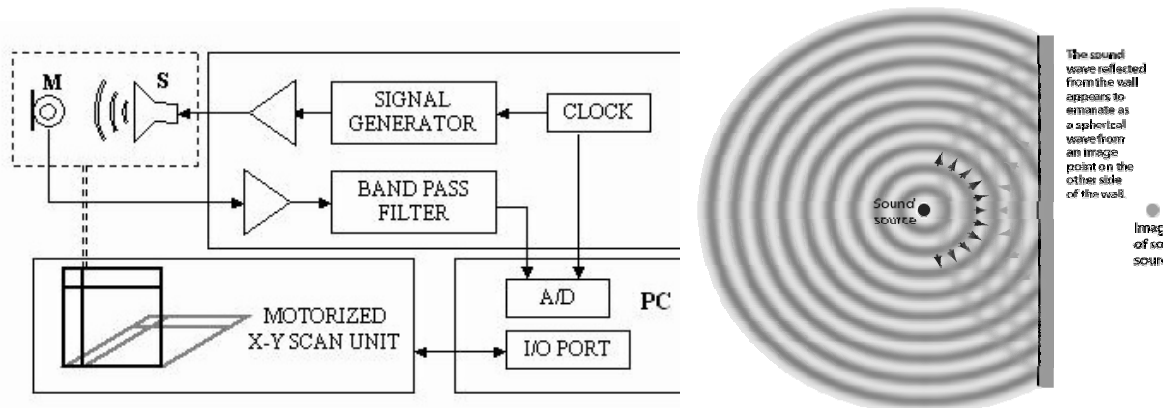4- _data acquisition, signal processing_ and _scan unit control_.

Figure 7: Scheme of the ACEADD device (left), and reflection of a spherical acoustic wave by a rigid wall (right)

The method employs a wide band sine wave sweep, with flat frequency band containing the expected resonance frequencies of the system under investigation. It realizes the measure of the _normal incidence absorption coefficient α_ through the determination of the surface transfer function $H_s(\omega)$, the Fourier transform of the impulse response of the surface $h_s(t)$. For this purpose the _Cepstrum algorithm_ is used in the signal processing in order to allow a direct extraction of the impulse response $h_s(t)$. The acoustic pressure _p(t)_, detected by the microphone _M_ at a standard working distance of about 0.5 m from the surface, is the superposition of the incident wave $p_i(t)$ and the reflected wave $p_r(t)$. This last is the convolution of the incident wave and the impulse response, delayed by the echo delay time τ and corrected by a spherical spreading factor k_r, accounting for the different paths between incident and reflected waves:

$$p(t) = p_i(t) + p_r(t) = p_i(t) + k_r p_i(t) * h_s(t - \tau) \qquad (22)$$

where $k_r = L / (L + c\,\tau)$ and _L_ is the distance between source and microphone and _c_ is the speed of sound in air. The acoustic pressure _p(t)_ is processed by means of the Cepstrum algorithm mentioned above and set as the inverse

Fourier transform of the natural logarithm of the power spectrum of the measured signal, thus obtaining the *Cepstrum trace*:

$$C(t) = C_i(t) + k_r h_s(t - \tau) + \text{higher order terms.} \tag{23}$$

The algorithm transforms the second term in Eq. (22), representing the reflected wave, from a convolution to a simple sum of the impulse response in the Cepstrum trace, Eq. (23). Furthermore, for suitable acoustic waves and characteristics of the transducers and related circuitry, the contribution of the incident wave to the Cepstrum $C_i(t)$ is negligible in the vicinity of the echo peak, so that the surface impulse response emerges as an isolated and very narrow structure over a quite flat background. Assuming this conditions are met, the impulse response can be easily extracted by means of a window function W(t-τ), centered in τ :

$$h_s(t - \tau) = [C(t) - b.g.] W(t - \tau) / k_r \tag{24}$$

where the expected value of the flat background, b.g. in the equation, is zero. The transfer function $H_s(\omega)$ results from simply the Fourier transform of the impulse response obtained in Eq. (24), except for a multiplicative term due to the delay shift, and as a consequence the reflection coefficient *r* and absorption coefficient *α* are calculated as:

$$H_s(\omega) e^{i\omega\tau} = FFT[h_s(t - \tau)] \tag{25}$$

$$r_p(\omega) = H_s(\omega) \tag{26}$$

$$r(\omega) = \frac{1}{k_r^2} \frac{|P_r(\omega)|^2}{|P_i(\omega)|^2} = |H_s(\omega)|^2 \qquad \text{and} \qquad \alpha(\omega) = 1 - r(\omega) \tag{27}$$
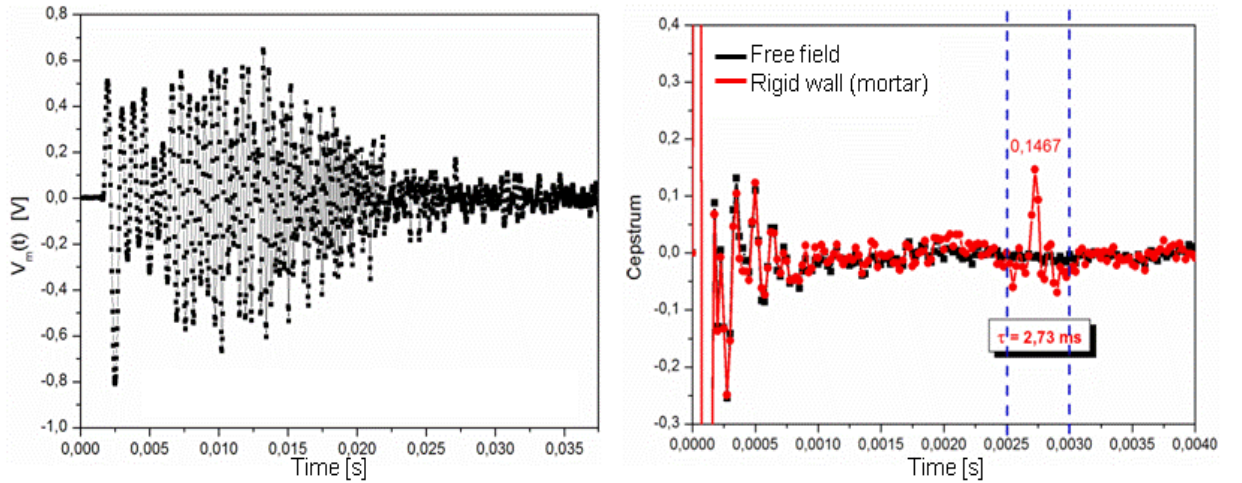
Figure 8: Incident and reflected waves (left);
Cepstrum traces with reflection peak, and in echo free conditions (right).

In principle, the method presented is useful to determine the impulse response, the reflection coefficient or the related surface impedance, as well as the energy reflection coefficient and absorption coefficient [15-17]. To detect decay in cultural heritage assets an *indicator* of the presence of absorption has to be selected among the above quantities in order to achieve the most complete indication about the deterioration of the object through the application of the simplest procedure. The aim is to save as much time as possible by avoiding redundant analysis without losing accuracy. For this purpose different indicators can be adequate with respect to different levels of understanding. First of all the analysis can be focused on the impulse response whose features denote the presence of acoustic absorption. A further step is the evaluation of absorbing processes regardless of their frequency dependence, since a certain amount of energy absorption is associated to the presence of cavities. These two analyses are quite straightforward and fast, since they apply directly to the impulse response after the windowing of the Cepstrum trace. The reflection peak height h_{max} can be extracted, in the first case, and the integral over the time window of $|h_s(t-\tau)|^2$ can be calculated, in the second case, that for the Parseval's theorem equals the integral over the frequency range of $|H_s(\omega)|^2$, i.e. the total amount of reflected energy. The result is associated to point coordinates and delay time, and collected into matrices that represent the input data for building acoustic maps. The ultimate level of analysis is realized obtaining for each point the frequency dependence of reflection coefficient or absorption coefficient, Eq. (27), with the extraction of the resonance frequency useful to determine the depth of the cavity. This last detail together with the extension of detachment, visible in the surface map, may help to define the geometry of the cavity.

At present some methods are internationally standardized for the measurement of the absorption coefficient, and are used to characterize and certify the acoustic performance of specific products; for instance the international standard ISO 354 [18] describes the measurement of the diffuse field absorption coefficient in the reverberation room, and the ISO 13472-1 [19] is commonly used for in situ characterization of road surfaces. Nevertheless these methods apply to homogeneous structures and materials or reveal the overall effect of an absorbing element, thus they are not suitable to characterize more complex and heterogeneous structures such as artistic heritage assets.

The system is illustrated in Fig. 9 with the XY scan unit, the linear scan unit, more flexible and suitable for many different configurations of the site, and the standard mounting configuration of the transceiver unit.

Figure 9: The ACEADD system: the scan units (top) and the transceiver unit (bottom).

7 - THE LOCATION

The Madre de Deus Convent is a Portuguese National Monument situated in Xabregas, on the western area of Lisbon. The Convent was originally built between 1509 and 1516, and houses nowadays the National Tile Museum (Museu Nacional do Azulejo - MNAz). The 16th century construction was affected by the earthquake of 1755 and the present building is a combination of 16th to 18th centuries architecture, with decoration motifs that span to the late 19th century.

Figure 10: The Madre de Deus Convent

.

The object of the investigation is the application of *in situ* acoustic diagnostics to tile panels. For the realization of the study two locations within the old conventual building where selected:

i)   the assessment of tile detachments from the wall used as test subjects two panels at the 18th century D. Manuel room, scheduled for a future conservation intervention and presently used on a temporary basis to house part of the extensive reserves of the museum inventory; and

ii)   the top level of the cloister, whose walls are covered with low set panels obviously affected by moisture and depicting extensive loss of glaze, attributable to a manufacturing defect, probably shivering.
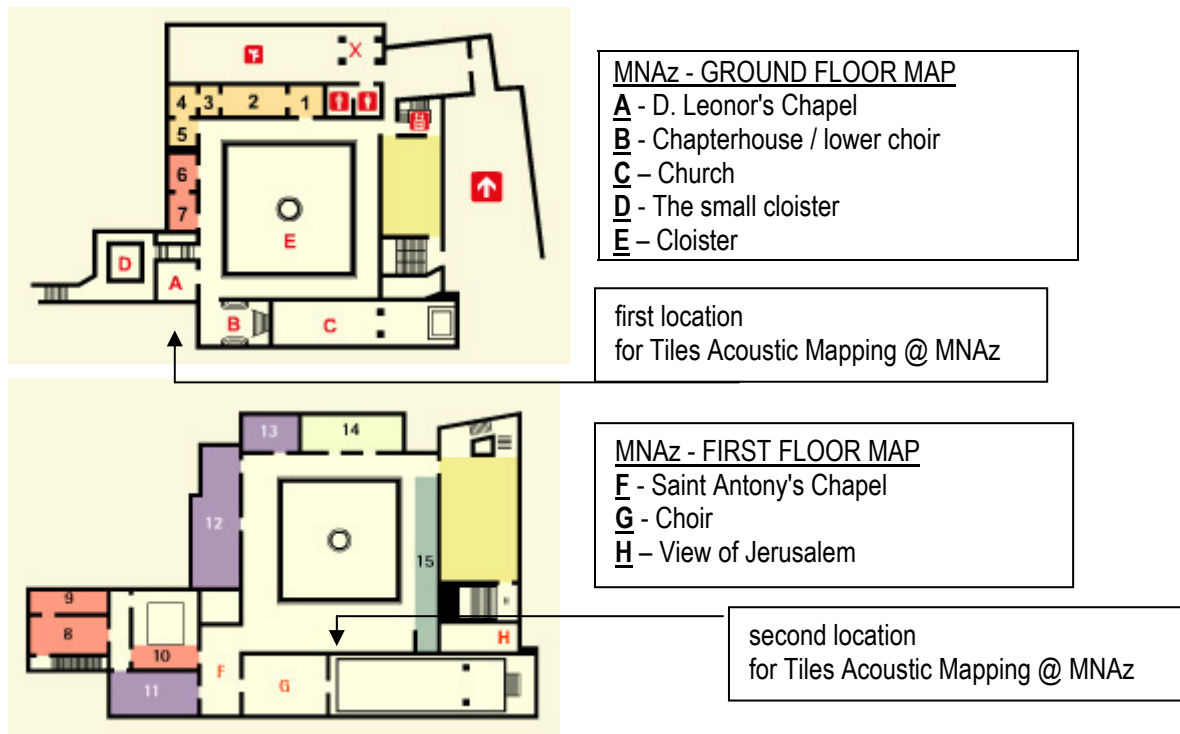
Figure 11: Locations at the National Tile Museum where in situ measurements were carried out.

A plant of the building is reported in Fig. 11, where the two locations described above are indicated. A number of panels, shown in Fig. 12, presenting interesting features for the study were selected in the two locations.

Figure 12: Tile panels selected for acoustic mapping at the first location (left) and at the second location (right)

8 - THE MEASURING PROCEDURE

The ACEADD diagnosis points to the realization of acoustic images whose measured quantity is related to the presence of detachments and delaminations. The output of the measuring procedure is a map; in particular the experimental data may be displayed as a 2D map and a 3D map of the absorption percentage. Furthermore, a 2D map overlaid on the image of the surface under investigation helps the operator in the localization of significant detachments, showing a number of thresholds applied to the absorption percentage that delimit the more damaged areas.

The measuring procedure consists of different operations, summarized as follows.

- PRELIMINARY TEST: NOISE evaluation, FREE-FIELD evaluation

Some *preliminary tests* aim at the characterization of the environment, and the characterization of the electronic chain. These tests take account of Noise evaluation, performing acquisition with the transmission not active, and of Free-Field evaluation, performing acquisition in active configuration with the system far from reflecting targets. The results are relevant in order to reproduce the best conditions for the Cepstrum algorithm work properly.

- TRANSCEIVER MOUNTING AND SYSTEM ALIGNMENT TO REFERENCE POINTS

The subsequent important step is the *arrangement of the transceiver unit* and the *alignment of the measuring system*. In particular the microphone is clamped to its holder at a particular distance from the acoustic source, so that the far field condition with the spherical spreading of the acoustic field is satisfied for both the incident and reflected wave. The scan unit, mounting the transceiver unit, is aligned with respect to the tile panel using a laser beam. The microphone is placed at a specific distance from the surface of the panel equating the source-microphone distance, so that the direct to reflected wave path ratio (equal to k_r) is not greater than 1/3 (required for the approximation in the Cepstrum algorithm became valid). Some reference points are selected in order to align the scan unit's graduate scale with the image of the tile panel. The perimeter of the scanned area and the reference points are marked on a digital image of the panel, so that the mesh of the measured absorption map can be superposed on the panel image.

- REPEATABILITY TEST

Once the measuring configuration and input parameters are chosen, the next step is to assess the *repeatability* of the measurement in order to evaluate the effectiveness of the diagnosis and the reliability of the experimental results. Some details about this point are discussed in section 9.1.

- ACEADD MEASUREMENTS: ABSORPTION MAPS

Once all the preliminary tests are completed, the measure of the absorption coefficient is realized by means of a scan in a plane parallel to the surface under investigation. The scan follows the mesh previously identified; for this purpose the points of a matrix and the step size are defined.

The input signal is a logarithmic sine sweep with a frequency band suitable for detachment or delamination resonance excitation. For each point the system acquires a number N of acoustic pressure time histories and processes the signals in order to collect the whole Cepstrum trace and extract the absorption indicator (impulse response height h_i, or the total energy Σ_i). In Tab. 7a and 7b a scheme of the input and output quantities is reported.

For all the tests a general purpose board controls the signal generation, the acoustic pressure acquisition from the receiver, and the movements of the automated scan unit, as shown in Fig. 13. For the determination of parameters, relevant for the calculation of the impulse response, and for the evaluation of the sensitivity of the method to the environmental condition, an environmental parameters monitoring system usually completes the experimental apparatus. In this study a Mikromec Multisens logger, equipped with temperature and relative humidity probes, was used.

- ACOUSTIC IMAGE ELABORATION

The last step is the elaboration and presentation of the experimental data as acoustic maps. The values of the indicator are calculated with respect to the maximum value of a highly reflecting point, or the value obtained on a reference totally reflecting material. In any case the results indicate the percentage of energy absorbed by the area of the object under study.

INPUT QUANTITIES		
Image of panel surface, Perimeter of analyzed area, Reference Points		
Matrix definition: N° of Lines, N° of Points per line, Step [mm]		
Distance between the Source S and the Receiver M $d_{s\text{-}m}$[m]		
Transmission	SW1: 100Hz ÷ 10kHz, 1V amplitude	
	Ln Sweep, minimum phase filter ON	
	500kHz sampling rate, 10ksamples	Tile Detachment
	SW2: 5kHz ÷ 20kHz, 1V amplitude	
	Ln Sweep, minimum phase filter ON	
	500kHz sampling rate, 10ksamples	Glaze Delamination
Recording	40kHz sampling rate, 1,5k samples, 100 averages.	
Ambient Temperature	T_{amb}[°C]	
Limits of Time Window for impulse response extraction	t1[s]; t2[s]	

Table 7a: Input quantities in ACEADD measurement.

OUTPUT QUANTITIES
Rough data: N pressure time histories
Processed data: averaged pressure time history; averaged cepstral trace;
Output Matrix: for ith point $[X_i,\ Y_i,\ h_i,\ \tau_i,\ \Sigma_i,\ d_i,\ k_i,\ \alpha_i(f)]$

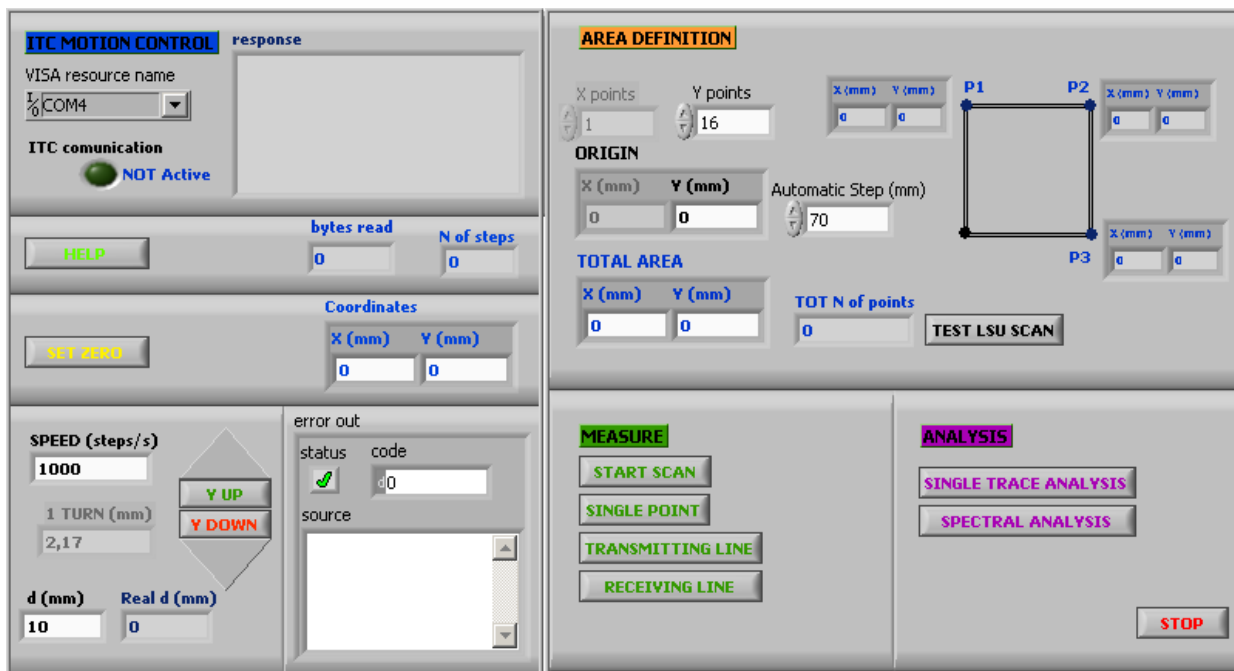**Table 7b:** Output quantities in ACEADD measurement.

Figure 13: Front panel of the software package, specifically configured in National Instruments' LabView environment for the ACEADD system.

9 - DATA ANALYSIS

The *in situ* investigation of deterioration in glazed ceramic tile panels was oriented to assess the reliability of the acoustic method for both tile detachments and glaze delaminations. For this purpose three maps for tile detachments and three maps for glaze delaminations were realized at MNAz, as described in section 6. General information about the identification of maps, the frequency band of the input signal, the number of lines and points and step size for each output matrix, with the total number of points are summarized in Tab. 8.

In the following subsections the results from the repeatability test and the six acoustic maps are presented, dealing tile detachments and glaze delaminations separately. Furthermore, for the validation of the acoustic method, a map obtained by means of *martelletto* evaluation were realized by LNEC researchers and compared with the absorption map of the same panel

ACEADD MAPS		
ACEADD MASUREMENTS: Tile Detachments	**MAP NMA1** [100-10k] Hz	[13L × 18PTs], 50mm step; 234PTs
	MAP NMA2 [100-10k] Hz	[24L × 21PTs], 50mm step; 504PTs
	MAP NMA3 [100-10k] Hz	[31L × 16PTs], 70mm step; 496PTs
	MAP NMA4 [5-20] kHz	[20L × 39PTs], 10mm step; 780PTs
Glaze Delaminations & Defects	**MAP NMA5** [5-20] kHz	[17L × 21PTs], 10mm step; 357PTs
	MAP NMA6 [5-20] kHz	[6L × 13PTs], 10mm step; 78PTs

Table 8: Scheme of ACEADD measurements carried out at MNAz.

9.1 - Repeatability of measurements

An accurate determination of the acoustic diagnostics effectiveness requires an evaluation of the precision of measurements. In the International Vocabulary of Metrology – VIM [20] the measurement precision is defined as the closeness of agreement between measured values of a quantity obtained by replicate measurements on the same or similar objects, under *specified conditions*. It is used to evaluate *measurement repeatability*, *intermediate measurement precision*, and *measurement reproducibility*. In particular the VIM defines the above specified conditions as:

REPEATABILITY CONDITION OF MEASUREMENTS
Condition of measurement that includes the same measurement procedure, same operators, same measuring system, same operating conditions and same location, and replicate measurements on the same or similar objects over a short period of time;

INTERMEDIATE PRECISION CONDITION
Condition of measurement that includes the same measurement procedure, same location, and replicate measurements on the same or similar objects over an extended period of time, but may include other conditions involving changes (the changes can include new calibrations, calibrators, operators, and measuring systems);

REPRODUCIBILITY CONDITION OF MEASUREMENT

Condition of measurement that includes different locations, operators, measuring systems, and replicate measurements on the same or similar objects (the different measuring systems may use different measurement procedures).

Indeed the repeatability evaluation is the first step to assess the degree of closeness between a certain number of independent replicates, thus a part of *in situ* experimental tests was oriented to assess this feature. The tests were performed carrying out four independent acquisitions of two selected vertical lines on the analyzed panels, collected in a few days time spread, following the same procedure used for the maps. For each repetition the system was re-configured, i.e. LSU re-positioned and TRU re-assembled in order to account for random error, while the measurement procedure, the system and the references for tile-system alignment were held unchanged. These tests were performed in the first location in MNAz, where the environmental parameters remained quite stable. For this reason differences due to environmental changes could not be appreciated. For the analysis the *mean value*, the *standard deviation*, and the *standard deviation of the mean* of the replicate measurements were calculated taking as indicators both the impulse response peak height and its energy content. For this analysis unfiltered data were used, thus resulted in higher standard deviation values with respect to that from filtered data. A summary of the analysis is reported in Annex 3. Even though this represents only a first evaluation of repeatability on rough data, the results show that the dispersion of values referred to the reflection peak in the Cepstrum trace is comprised in less than 4.5% relative standard uncertainty for most points for NMA3_L11 and 8% for NMA2_L15. Taking the impulse response energy as indicator, the replicates result in less than 8% for NMA3_L11 and 17,5% for NMA2_L15. The higher values are due to the higher noise of unfiltered data that enhances the values in the integration. Furthermore, looking the four replicate lines, it results that the system position can be properly reproduced. The correlation functions between the four replicate signals were analyzed, for a single point in NMA2_L15, shown in Fig. 14. The correlation between each replicate signal and its direct input signal, acquired in the free field conditions, was calculated. The curves show a very high degree of correlation between the replicates that equals the autocorrelation function, both for the direct peak and the reflection, visible at Lag 90. The height and the position of the reflection in the four independent replicates are reproduced very accurately.
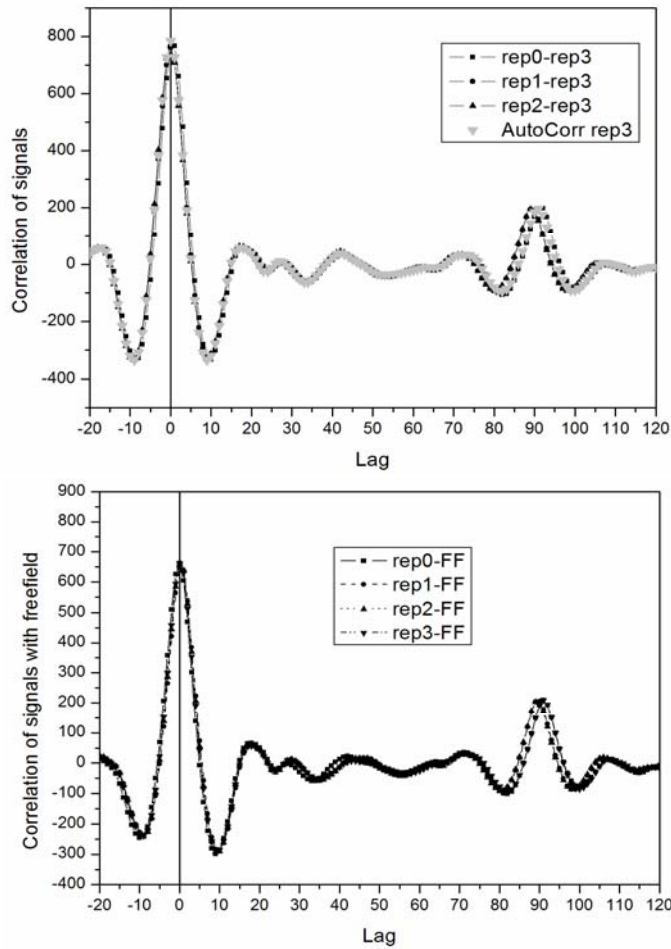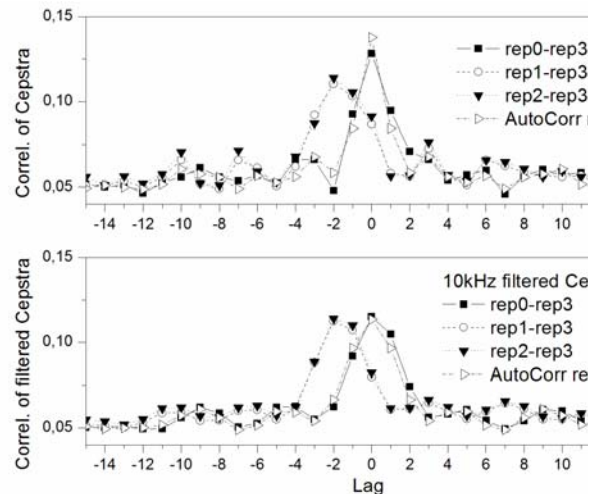
Figure 14: Correlation functions between the replicates of point Pt10 in NMA2_L15 (left) and between each replicate and the direct signal in the free field acquisition.
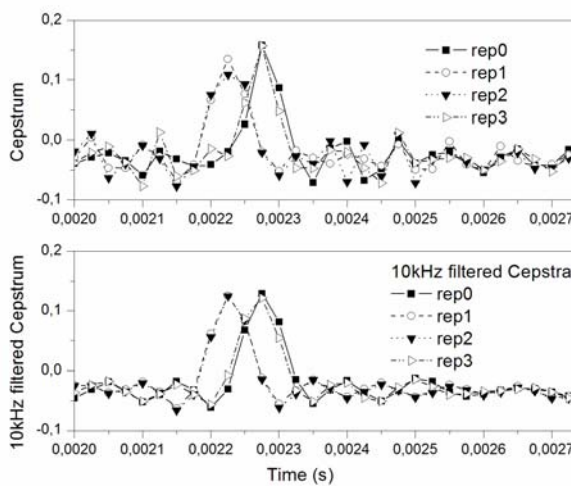
**Figure 15:** Impulse response in the Cepstrum replicates of point Pt10 in NMA2_L15.

Figure 16: Correlation functions between the replicates of impulse response in the Cepstrum trace of point Pt10 in NMA2_L15.

The correlation between the impulse response in the Cepstrum trace of the four replicates was analyzed after the application of a window function, showing a little shift of two peaks and the difference in peak's height, also visible in the entire lines reported in Annex 2. These differences are present both in the reflection

peaks and in their correlation functions, as shown in Fig. 15 and Fig. 16, disappearing after low-pass filtering with cut-off frequency set at 10 kHz, the high frequency limit of the transmitted signal frequency band. It indicates that the characteristic features of the impulse response (height and shape) are exactly reproduced after noise reduction is applied.

An ultimate verification was performed on the absorption coefficient curves of the four replicates, as shown in Fig. 17. The curves present a quite good agreement in particular at the low frequency maximum around 250 Hz, even if an unphysical minimum emerges at 1250 Hz. It might be due to spurious reflection effects or to vibrations of the transceiver unit's mounting that affect the measurement of the reflection coefficient, thus resulting in a value above unity.
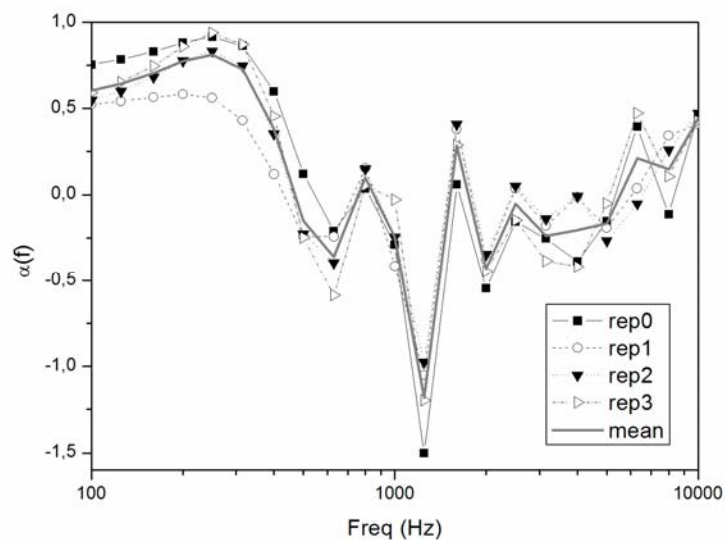
Figure 17: Absorption coefficient, calculated in 1/3 octave band, of the replicates at point Pt10 in NMA2_L15

9.2 - The experimental results

In the following sections the acoustic maps realized in the selected locations at MNAz are presented and the most relevant aspects related to different levels of interpretation are discussed.

The acoustic images of the panels were obtained following the experimental procedure described in Section 8. Since glazed ceramic tile panels present in plane discrete and periodic organization of unit elements, the tiles, a reasonable mesh size can be determined by tile size, beyond the characteristic spatial resolution of the device (better than 50 mm) and the required degree of details description. A proper choice can be a fraction of tile size so defining the minimum number of points properly representing the status of the object. Thus, observing the common fracture profiles occurring in tiles, the mesh unit cell and relative matrix step can be half the tile size, for instance four points per tile, with points centered in each quadrant as shown in Fig. 18. This criterion defines the suitable number of points in the map to achieve a representative picture of the analyzed

surface avoiding redundancy, reducing the acquisition time. In this case alignment and position reproducibility become crucial, and the alignment procedure must be carefully carried out. For glaze delaminations and small defects, the previous criterion does not allow an adequate detailed picture of the surface thus a smaller mesh size is preferable down to 10 mm or less, even if integration over a wider area is expected.

Figure 18: Fracture profiles in single tiles at the first location, and point arrangement for acquisition.

The collected data are here displayed using the total reflected energy as indicator, and extracting the absorption percentage with respect to a reference point, that is the point of the map showing maximum reflection. In this case the measurements can be assumed to be relative measurements, for which less stringent requirements about device calibration are needed. Afterward, the experimental results are discussed employing different tools, focused on peculiar aspects, all contributing to a comprehensive diagnosis of the artifact.

9.3 - Detachments

Three wide area acoustic maps, NMA1 NMA2 and NMA3, were realized at location 1 at NMAz. The location offered very stable environmental conditions for the measurements, and the almost private fruition of the room, closed to visitors, guaranteed noise limitation. The only possible sources of noise were external to the building, ascribed to human activities from the adjacent road and railway.

Assuming that in most cases a priori knowledge of the surface acoustic behavior is not possible or required, a first analysis can be based on the dispersion of values in a defined area of interest. This level of interpretation gives information about the *degree of heterogeneity* of the surface, with respect to the acoustic behavior of matrix points. The analysis includes a comparison of the dispersion of values of the collected data, representing an area of interest, with respect to the standard deviation *s* obtained in the repeatability test, regardless of point arrangement. The standard deviation is an evaluation of the resolution for the specific measurement, so that values falling inside an interval *2s* cannot be discriminated. From the replicates collected in the repeatability test, in particular those taken in the same session with the instruments in their steady state, representing the measuring conditions for a whole map, typical values of standard deviation are less than 10% for NMA2 and less than 16 % for NMA3 with unfiltered data set. Looking at the histograms of Fig. 19 for the three maps, where

the values are spread over a number of intervals 0.005 wide, one may expect that the indicator's values gather in a restricted interval around a central value in a uniform surface, while a wider range of values is expected from a rather heterogeneous surface with a reasonable presence of damaged areas. In NMA1 the central value is about 0.095 and the full width at half maximum FWHM is about 0.040 (8 bins), while the expected spreading of values for a uniform surface would be at least 0.030 (6 bins). For NMA2 a similar situation occurs: the central value is about 0.100 and the FWHM is about 0.035 (7 bins), while the expected spreading of values for a uniform surface would be at least 0.020 (4 bins). In these maps a consistent number of points constitute the tails of the distributions, in particular the right hand tail representing the most reflecting part of the surface. For NMA3 a different situation emerges: the central value is about 0.070 and the FWHM is about 0.020 (4 bins), well beneath the expected spreading of values for a uniform surface equal to about 0.022.
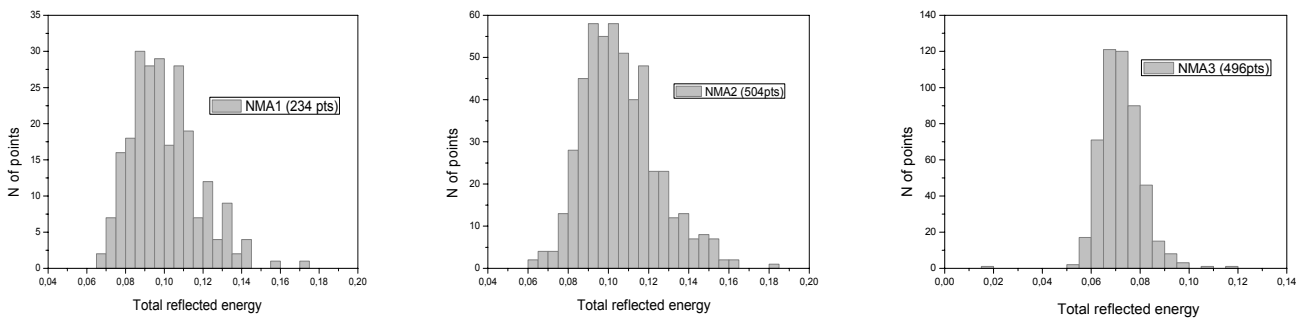
Figure 19: Dispersion of indicator values in NMA1, NMA2, NMA3.

As a result, map NMA3 presents a quite homogeneous acoustic behavior, while map NMA1 and map NMA2, belonging to the same panel, present a more heterogeneous behavior. How much heterogeneity is related to a deterioration state, and how much homogeneity guarantees a good state of the surface under investigation, depends on how distant the central value of the distribution is found from the *total reflection value*. In the present study the most reflecting point is used as the reference point, and its indicator's value is therefore assumed to be the best estimate of the total reflection value. But this is not in principle true unless an accurate calibration of the device is accomplished and the frequency analysis confirms this assumption.

Since at this level of interpretation the analysis is purely statistical, particular attention has to be paid to the number of points constituting the data set and to the typology of wave excitation, in particular to the width of the frequency band. For a sine sweep signal the wider is the frequency band, the higher is the number of detachment that can be excited and revealed. In NMA1, NMA2 and NMA3 the excitation presents a wide frequency band (100 Hz:10 kHz) enhancing the probability to excite detachments with different cavity depth. Nevertheless the

probability to directly discriminate different degrees of deterioration is reduced and an accurate frequency analysis becomes compulsory.

Acoustic maps provide extended views of the analyzed areas giving evidence to differences in acoustical behavior between points. The aim of acoustic mapping is therefore the *localization* of most absorbing points, related to detachments and delaminations, for which the importance of map alignment to the surface under test becomes evident. Since the maps display absorption percentage with respect to the most reflecting point of the map, a confirmation of the reference point as highly reflecting point is required. Real surfaces with damaged parts, or the proximity of particular architecture elements and edges may affect the measure introducing spurious reflections or diffusion, or altering the effect of the spherical spreading of the waves. The point for which the indicator's maximum value is found is considered a reliable reference point only if the reflection coefficient shows almost constant dependence on frequency and the value approaches unity. Frequency analysis is therefore required to direct the choice of the reference point in each map. Fig. 20 and Fig. 21 show map NMA1 and map NMA2 respectively; both maps belong to the same panel and present similar conditions, quite large areas showing absorption even though not extremely high. The panel is also shown in Fig. 23 with map NMA1 and NMA2 overlaid on the panel image, where three thresholds are set at 30%, 40% and 50% of absorption to give evidence to the most deteriorated areas. On the basis of previous experience the selected thresholds are significant for discrimination between damaged and undamaged areas. Taking into account these evidences, it can be assessed that the panel presents an important portion of the coverage detached from the wall. The wide frequency band does not allow identifying at this stage the depth of cavities but only the extension, hence the comprehensive evaluation of the degree of deterioration is not possible until resonance frequencies are extrapolated.

A map of the same panel was also produced by using a percussion (knocking) technique similar to the martelletto. As respects to azulejos, the percussion technique must now be revised. Basically, the physical principle is similar to that of the acoustic diagnostic method, when a tile is detached it loses surface contact with the wall, forming a resonance chamber. When hit sharply, the sound perceived by the operator will vary according to the acoustic resonance of the system thus formed. As described above, the resonant frequency will be lower as the distance from the wall increases. In practice the situation is much more complex - a totally detached tile that is still in full contact with the wall will return a "non-detached" sound. On the other side, tiles are frequently detached in large patches of many azulejo units and thus hitting any tile of the group will actually excite the same resonant volume but at a different spot, accounting for the tonal differences. Detachment maps of azulejo panels may be achieved by deciding on a 1 to 5 scale of decreasing perceived frequency and judging the sound returned

when hitting any single tile in a given manner. The results must, however, be interpreted in the following way:

- a tile marked "1" is very likely fully attached, but it may conceivably be detached and still totally in contact;
- tiles marked "2" to "5" are detached and those with a higher "detachment rating" are either further away from the wall, or else they mark the center of a large detachment area.

Figure 22 shows the graphic result of an assessment of an area of the panel, shown in Figure 23, in which green corresponds to an assessment of "1 - fully attached" and red corresponds to an assessment of "5- detached and furthest away from the wall".

However, the maps in Figures 20, 21 and 23 cannot be compared directly with Figure 22, since the first are obtained with a measurement of a specific physical quantity, the acoustic absorption coefficient, which must be put into relation with the presence of resonant cavities in the specimen. The map in Figure 22 contains a subjective and interpretative analysis about the degree of detachment from the supporting wall, together with the application of a smoothing operator. For this reason differences are to be expected.

Figure 25 shows map NMA3, a quite wide area presenting isolated points with good adherence in a quite uniform state. An extended vertical region of slightly higher absorption appears in the centre, corresponding to the contour of the lower part of the cross. The left hand vertical line (line 1) is not very reliable due to border effects affecting the measurement. Furthermore the point of maximum indicator's value is placed in a very lateral region that can be affected by border effects. This point, as for the other two maps, is not a proper choice for an accurate adjustment of the color scale. Thus the reference point was selected on the basis of frequency analysis, as described before. Looking the acoustic map, the homogeneity of NMA3 is confirmed, as the histogram in Fig. 19 has evidenced.

The most comprehensive examination is represented by frequency analysis for which the absorption coefficient or equivalently the reflection coefficient is calculated as a function of frequency. Resonance frequencies related to detachments and delaminations can be determined, and cavity depth can be evaluated from the following equation

$$d(f_0) = \left(\frac{c_0}{2\pi}\right)^2 \left(\frac{\rho_0}{\rho_S}\right)\frac{1}{f_0^2}. \tag{28}$$

The most important aim of the frequency analysis is indeed the *determination of resonance frequencies* and the *evaluation of cavity depth*. Once the extension of

defects and its depth are obtained by means of acoustic mapping and frequency analysis, an advanced comprehension of the degree of deterioration of the panel is achieved.

The results are presented in Fig. 24 for a number of relevant points in NMA1 and NMA2. The analyzed points are marked on the panel image with maps superposition, while the reflection coefficients of some absorbing points (identified by *A* and a sequential number) are compared to that of the most reflecting points (identified by R and a sequential number). The reflection coefficient curves are chosen and displayed in such a way to give evidence to the absorption lines and their resonance frequencies. For this purpose, the impulse response in the cepstrum trace is windowed between the end of the direct wave cepstrum tail and the occurrence of the second order reflection peak at 2τ, Fourier transformed and the square modulus computed. The width of the time window determines the low frequency limit in the reflection coefficient and absorption coefficient. Once the time window is selected, its width must equal at least half a period of the lowest detectable frequency; in this case the low frequency limit is about 210 Hz. As it can easily seen in the graphs of Fig. 24, the reflecting points R1 and R4 are not suitable choices for the reference point selection. These two points presents the indicator's higher values for the two maps, but their reflection coefficient shows a great variability very far from total reflection behavior. The analysis confirms point R2 and point R5 more suitable as reference points in NMA1 and NMA2 respectively. For the other points in the maps the reflection curves show evident minima at specific frequencies. In Tab. 9 these resonance frequencies are reported together with the evaluated depth of detachment. The values of cavity depth are calculated assuming sample P5, already used in section 4.6 for expected resonance frequency values, as a representative tile model for the panels under examination. Thus being ρ = 1,75E+3 kg m^{-3} the tile density, t = 1,0E-2 m the tile thickness so that ρ_s= 17,5 kg m^{-2} is the tile mass per unit area, being ρ_0 = 1,292 kg m^{-3} the air density and c_0 = 343 m s^{-1} the velocity of acoustic waves in air, and using the experimental values of resonance frequency f_0, the cavity depth d is determined by Eq. 28.

The values of cavity depth range between few millimeters down to few microns, but some caution is required. The lowest resonances found at about 250 Hz are very close to the low frequency limit and the minima may be affected by the decaying profile of the curves, thus the measure of the frequency taken at minimum may be altered. At the high frequency limit very thin cavities are found, less than 10 μm, but in this range also glaze delaminations may occur, as the expected frequency evaluation of section 4.6 clearly shows.

MAP	Resonance Freq	Points	Cavity depth
NMA1	244 Hz	A5	3.7 mm
	390 Hz	A1	1.5 mm
	628 Hz	A3	0.56 mm
	2756 Hz	A5	29 µm
	(6300 ÷ 6536) Hz	A1, A2, A3	(5 ÷ 6) µm
NMA2	250 Hz	A6, A8	3.5 mm
	1395 Hz	A7	1.1 mm
	(7500 ÷ 7800) Hz	A8, A9	(3 ÷ 4) µm

Table 9: Evaluation of cavity depth from resonance frequency values, applied to sample P5 [8] taken as a representative example for the panels under investigation.

It has to be noted that there is a frequency band where the indication of very thin tile detachments may be mixed with that of glaze delaminations. If resonance frequencies around 6 kHz were ascribed to glaze delaminations, correspondent cavity depth would be about 50 µm, as shown in Tab. 6, that is a quite severe delamination equaling about 17% of glaze thickness. The visual inspection suggests that glaze delamination does not seem to affect the panels at location 1, nevertheless the question if such a thin tile detachment is really detectable or if it appears as a practically rigid structure still remains. A more accurate measurement based on a higher number of replicates would help to confirm the existence of such high frequency resonances.

The analysis on map NMA3 is not applied on single points among the most reflecting and the most absorbing ones, but on a complete row in order to examine the effect of a rather homogeneous condition throughout the panel on reflection coefficient profiles. Fig. 26 shows the reflection coefficient of all points in row 15, grouped in three sectors, with the reference point profile separating the low frequency band from the high frequency band. Very few points presents resonances, in particular they belong to the lateral sectors (lines 1 to 10) and (lines 21 to 31), while the central sector (lines 11 to 20) shows a group of very homogeneous and reflecting profiles with only a general decrease spread around 6400 Hz, corresponding to a potential cavity less than 6 µm deep.

One hypothesis is that a wide area of five or six tiles, still in contact between them, presents a very thin detachment. A second hypothesis is the presence of delaminations such as for the high frequency resonances in map NMA1 and map NMA2, hence the same note must be recalled in this case too. In Tab. 10 are reported the resonance frequencies found in row 15, the relative points identified by the number of line, and the evaluated cavity depths.

MAP	Resonance Freq	Points	Cavity depth
NMA3	250 Hz	L5, L7	3.5 mm
	(1500 : 2250) Hz	L2 to L5 L30, L31	(44 : 98) µm
	3700 Hz	L4, L5 L25, L30, L31	16 µm
	4250 Hz	L2, L4	13 µm
	5500 Hz	L31	7 µm
	(6000 ÷ 6800) Hz	L3, L17, L30	(5 : 6) µm

Table 10: Evaluation of cavity depth from resonance frequency values, applied to sample P5 [8]

As can be easily seen, most potential tile detachments are very thin having cavity depths below 100 µm that is 1% of tile thickness. Thus, the frequency analysis performed on map NMA3 confirms a homogeneous acoustical behavior throughout the surface and a general good state of conservation of the panel with only minor faults.
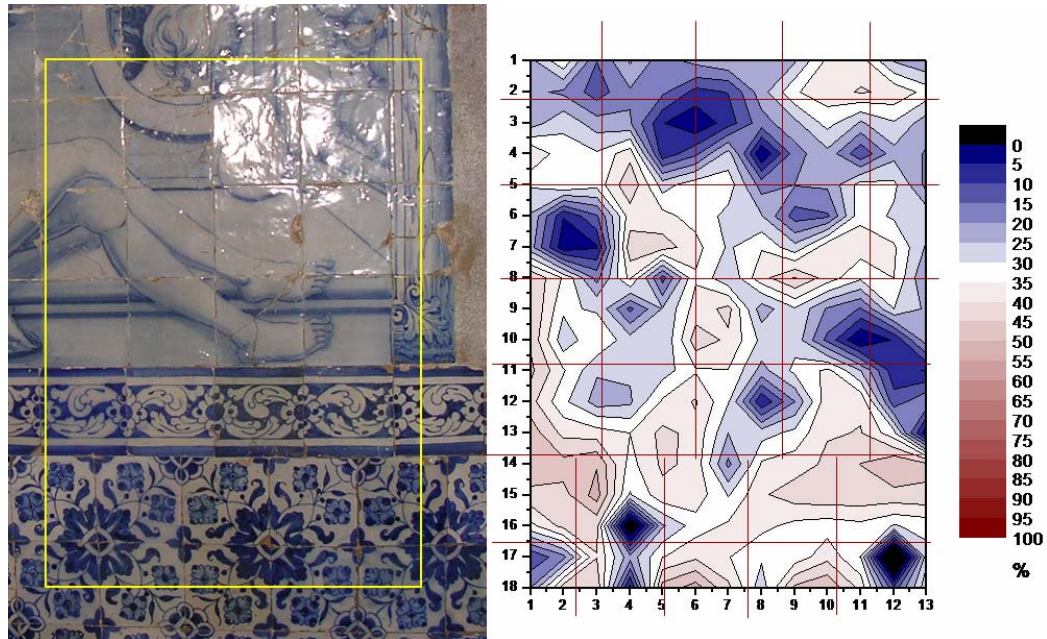
Figure 20: NMA1; Reference point is (8, 4).
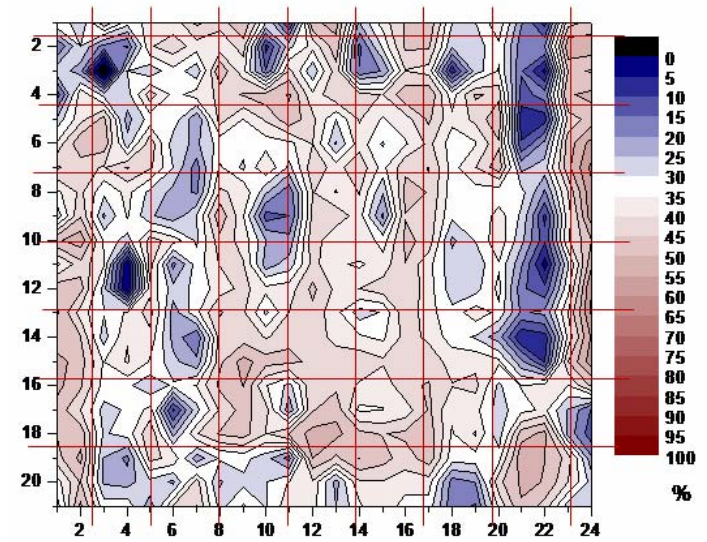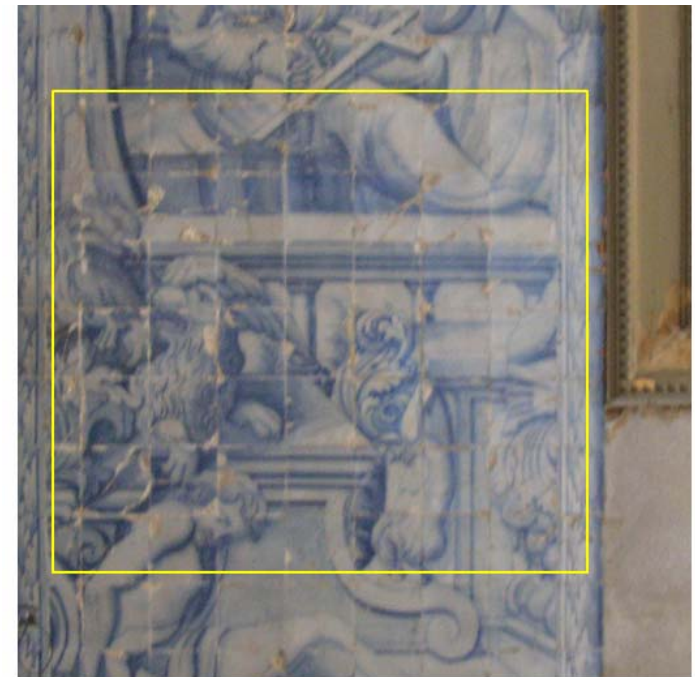
Figure 21: NMA2; Reference point is (4, 11).
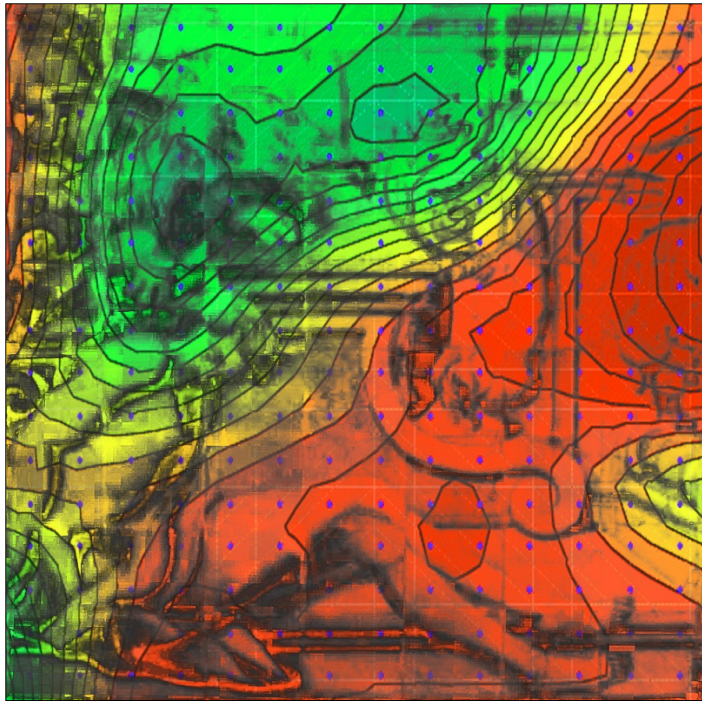
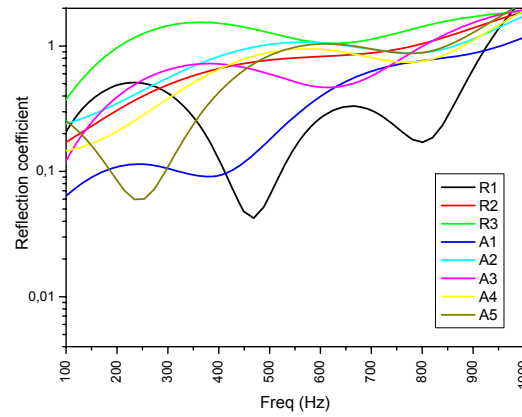**Figure 22:** Map detected by the *martelletto* (knocking) technique.
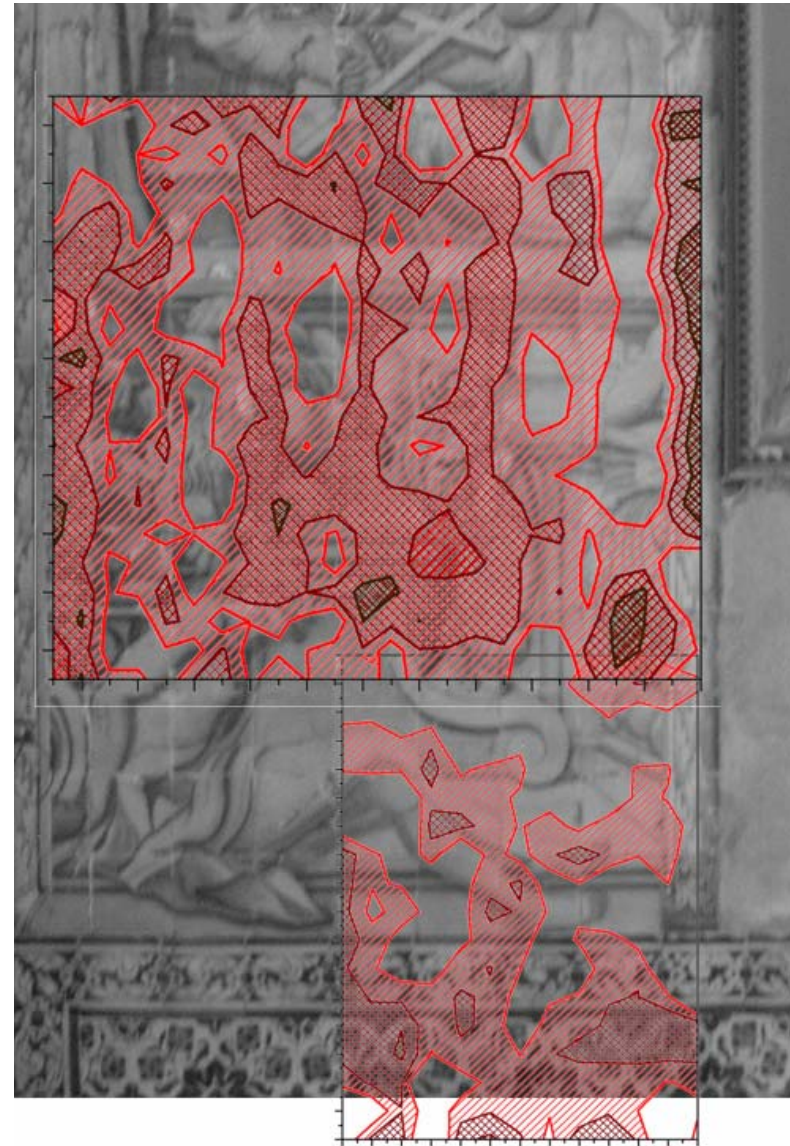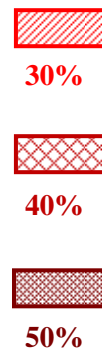
Figure 23: Combined NMA1 and NMA2 on the image of the first panel, where three thresholds are applied at 30%, 40%, 50%.
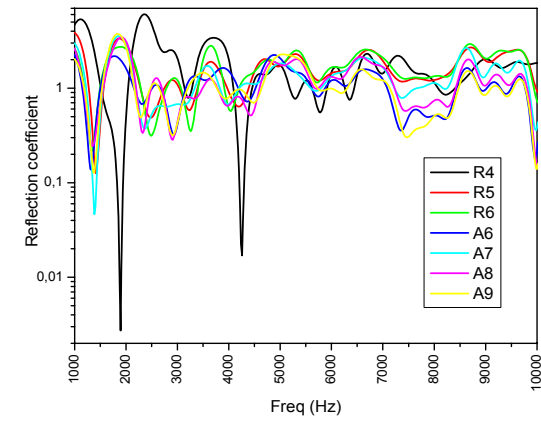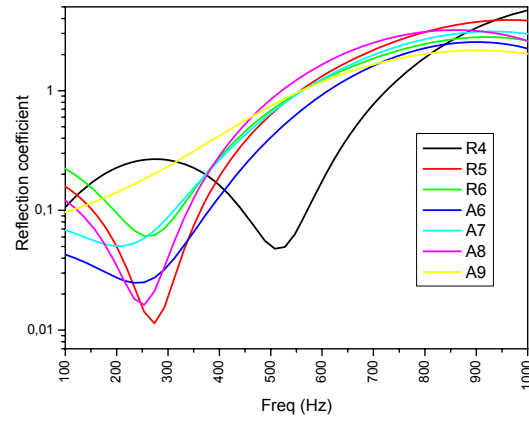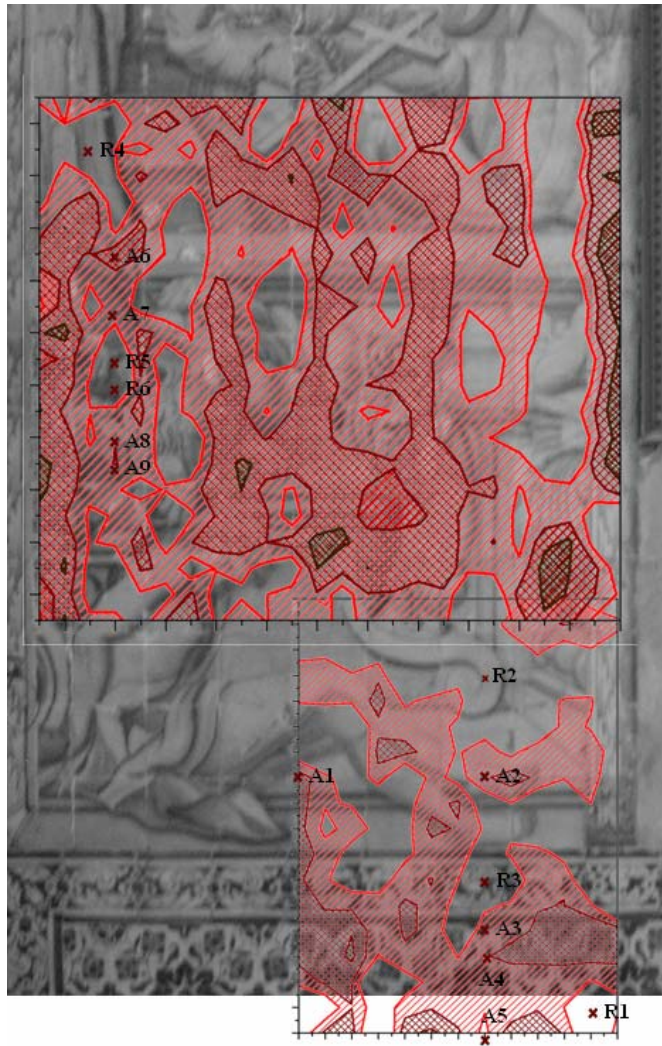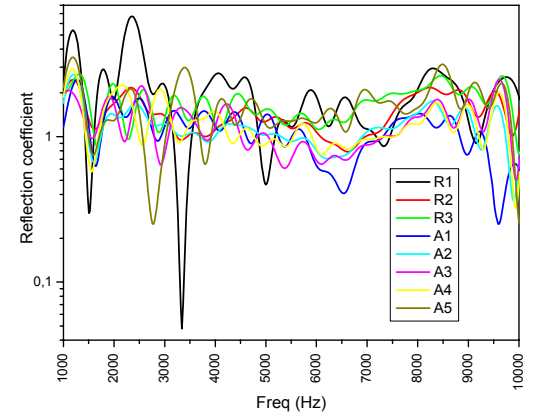
Figure 24: Frequency analysis applied to most relevant points of NMA1 and NMA2, with the points marked on the map. Reference points are R2 for NMA1 and R5 for NMA2.
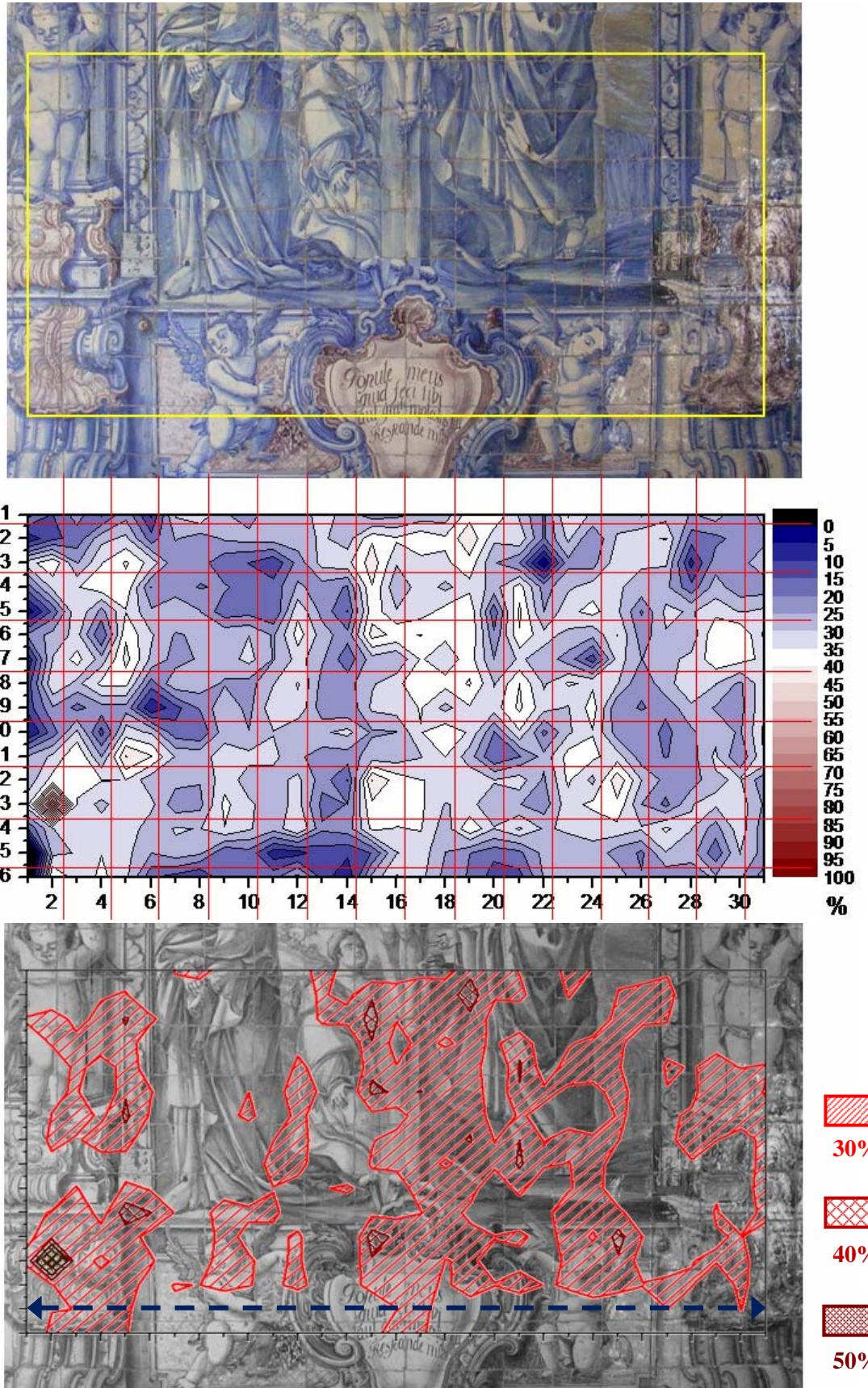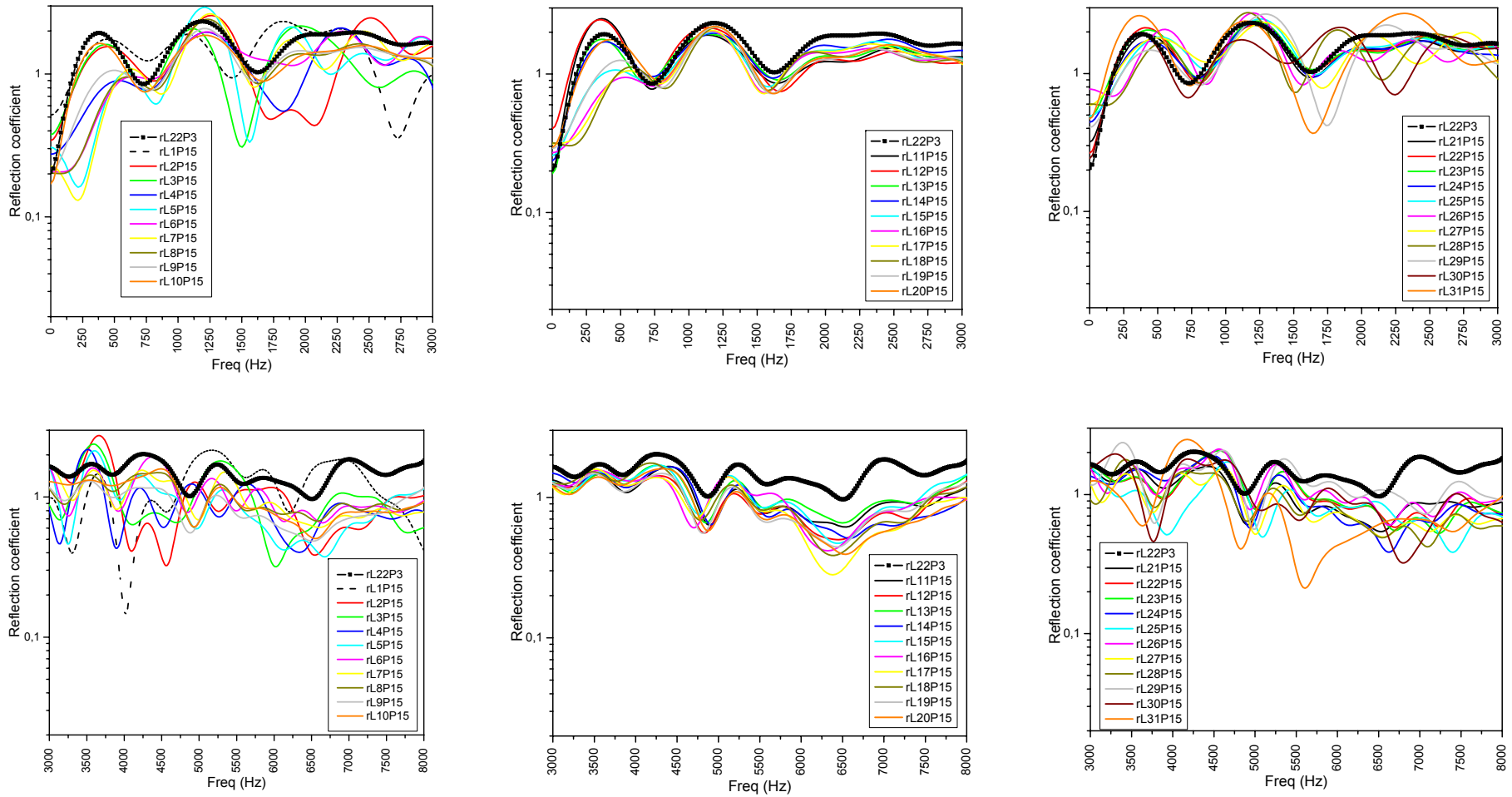
Figure 25: NMA3; the Reference point is (22, 3). The blue line marked on the bottom map indicates row 15, used in frequency analysis.

Figure 26: Frequency analysis applied to row 15 of NMA3, in the lower part of the map. The selected reference point for NMA3 is point (22, 3), while the point (1, 15) showing the highest indicator value does not present an adequate profile of highly reflecting point.

9.4 - Delaminations

Three small area acoustic maps, NMA4 NMA5 and NMA6, were realized at location 2 at NMAz. The location is part of the exhibition space in the upper cloister; although it was open to visitors the background noise did not affect much the measures. The environmental conditions were quite unstable with great temperature variation throughout the day, quite cool in the morning and hot in the afternoon because of sun exposure. The temperature was constantly monitored during measurements and its value was used for the correction to sound velocity. The azulejo panels, placed all around the cloister, are greatly affected by glaze delamination with high percentage of glaze loss, as shown in Fig. 27. Thus the measurements were directed towards the detection of delaminations at their very early stage of development.

Figure 27: Glaze delamination in azulejo panels located in the upper cloister at NMAz.

The acoustic excitation to reveal delaminations is restricted to high frequency band (5 kHz : 20 kHz), cutting off the characteristic low frequency absorption due to tile detachments. In order to obtain a detailed picture of the surface, a step of 10 mm was used, although the spatial resolution for this kind of diagnosis is well above this value and integration is expected. A repeatability test for these maps is not available, thus the wider deviation of 16% found for NMA3 to represent unresolved values is assumed also for these measurements. Fig. 28 shows the histograms from maps NMA4, NMA5 and NMA6. An important number of points build up the first map whose dispersion of values approaches a Gaussian profile: the central value is around 0.170 and the full width at half maximum FWHM is 0.045 (9 bins), while the expected

spreading of values for a uniform surface would be about 0.054 (11 bins). Map NMA5 and map NMA6 present a similar situation although the number of points in the two maps is very different. Anyhow they seem to broaden over a great interval with a peak showing not a very definite shape. For NMA5 the central value is about 0.150 and the FWHM is about 0.060 (12 bins), while the expected spreading of values for a uniform surface would be at least 0.048 (10 bins). For NMA6 the central value is about 0.145 and the FWHM is about 0.040 (8 bins), while the expected spreading of values for a uniform surface would be about 0.046 (9 bins).
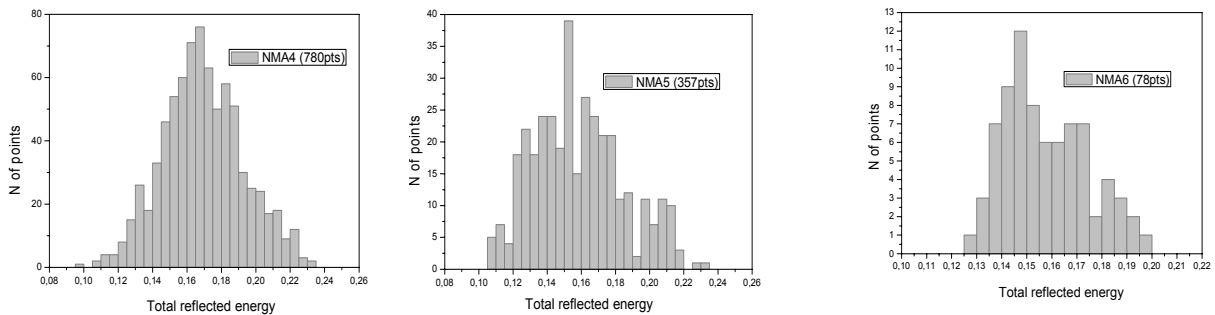
Figure 28: Dispersion of indicator values in NMA4, NMA5, NMA6.

In all maps a consistent number of points constitute the right hand tail of the distribution representing the most reflecting points. In map NMA4 and map NMA5 the left hand tail representing the most absorbing points are well outlined, while in map NMA6 the distribution is more asymmetric with a very little tail of absorbing points. From this analysis emerges that the first two maps present a slightly heterogeneous condition while the last map is characterized by a quite good homogeneity.

In these maps discrimination between points with and without glaze coverage, where the glaze is lost and the bisque is exposed, becomes relevant. In principle these areas can be discriminated since their absorption coefficient would show different features, but this aspect will be the object of further analyses.

Different kinds of map related to NMA4 are reported in Fig. 29; a sort of delimitation between adjacent tiles emerges from the absorption map of this area, containing a great number of boundaries with respect to NMA5 and NMA6. Exposed bisque is not clearly discriminated at this stage. The area present only few parts showing high absorption mainly localized in the four lower tiles, while the upper tiles seem to show no evident delamination but relevant glaze loss indeed.

NMA5 is essentially a map of a single tile whose state appears quite good at the visual inspection. Fig. 31 displays the measured absorption percentage for this map, revealing a different condition from the expected one, not in agreement with the visual analysis. The most absorbing areas correspond to the body of the figure leaving the upper half of the tile in quite good conditions, and the bottom of the adjacent tile at the top of the map.

Finally the last map realized at location 2, NMA6, depicts a very small area, quite uniform with some bubbles likely due to fabrication defects and not related to delaminations. Indeed the acoustic map, shown in Fig. 33, confirms the presence of very few absorbing points mainly on the left with very low absorption percentage, below 30% throughout the map. For this little map no particularly relevant note can be provided, other than a confirmation of the homogeneity emerging from the histogram in Fig. 28.

MAP	Resonance Frequency	Points	Cavity depth
NMA4	11060 Hz	A1	14 µm
	11850 Hz	A2, A3, A4	13 µm
	18800 Hz	A1	5 µm
NMA5	11500 Hz	A1, A2	13 µm
	14850 Hz	A1 : A6	8 µm
	(17750 ÷ 18270) Hz	A1, A3, A5	(5 : 6) µm
	19570 Hz	A4	5 µm

Table 11: Evaluation of cavity depth from resonance frequency values, applied to sample P5 [8] taken as a representative example for the panels under investigation.

In the examination of the reflection coefficient profiles, shown in Fig. 30 for NMA4 and Fig. 32 for NMA5, the selected reference points appear as adequate choices since highly reflecting behavior are clearly visible. The absorbing points in the two maps are characterized by evident minima. Few resonance frequencies are obtained and listed in Tab. 11. The evaluated cavity depths for both maps range from 14 µm down to 5 µm.

On the basis of these evidences the ACEADD method seems to be able to reveal the presence of cavities with depth down to few microns, hence it appears suitable for delamination detection even in the early stage of development. In principle, the limit of few microns could be overcome employing acoustic sources extended in the high frequency band. Anyway the comparison with other methods would help to define the upper limit in the resolution of the ACEADD device.
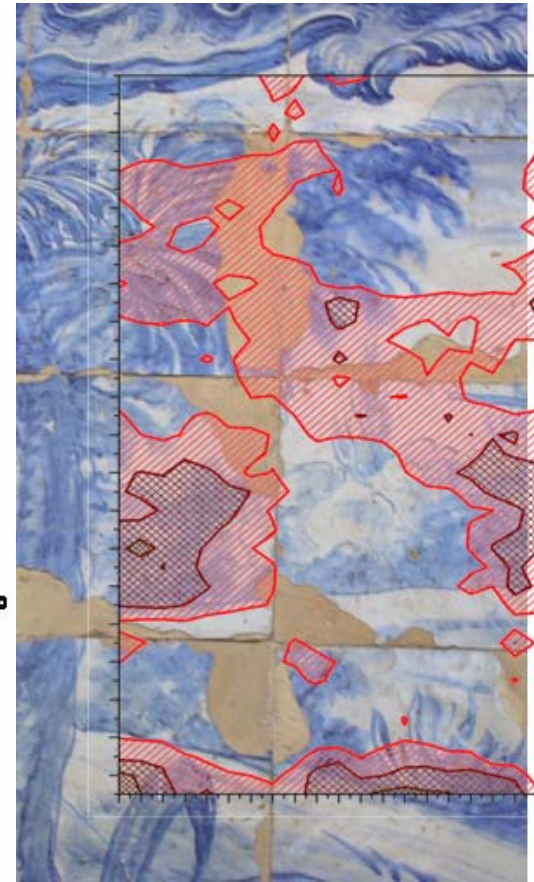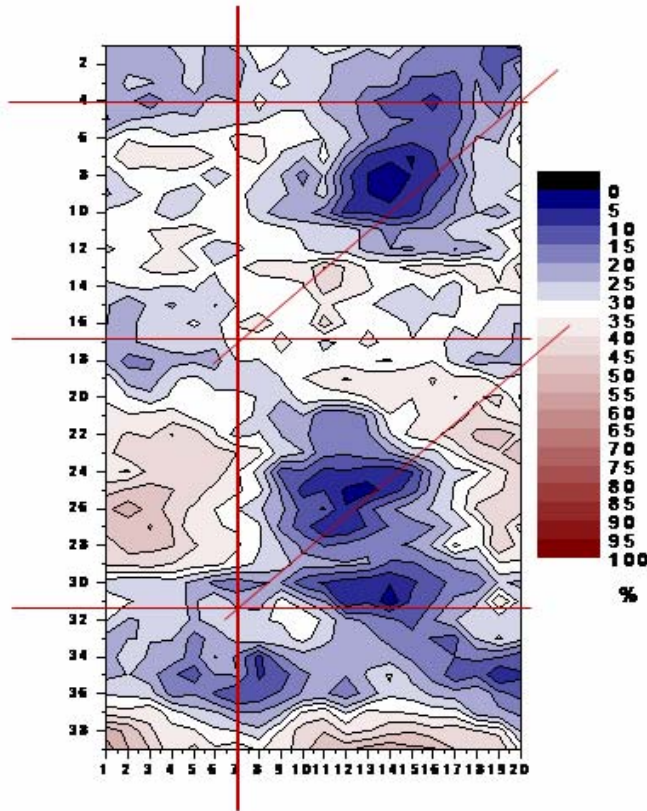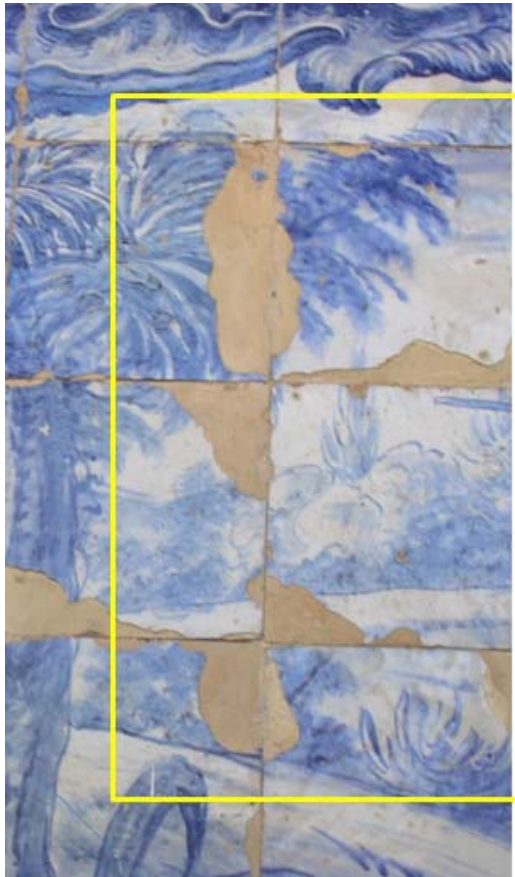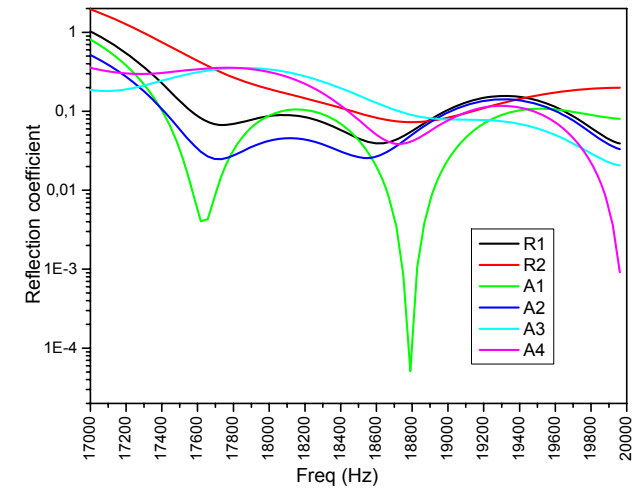
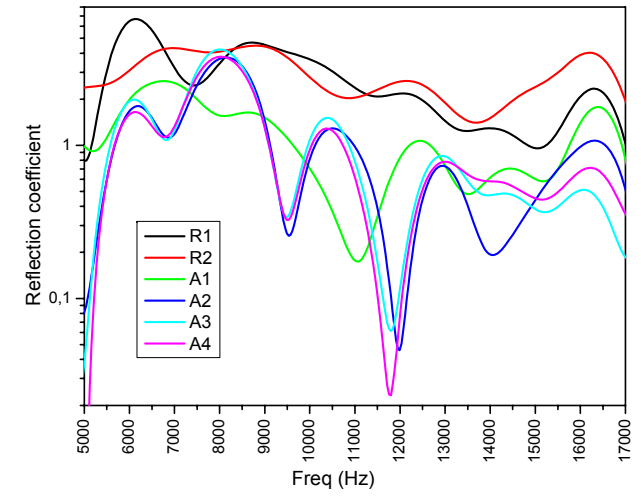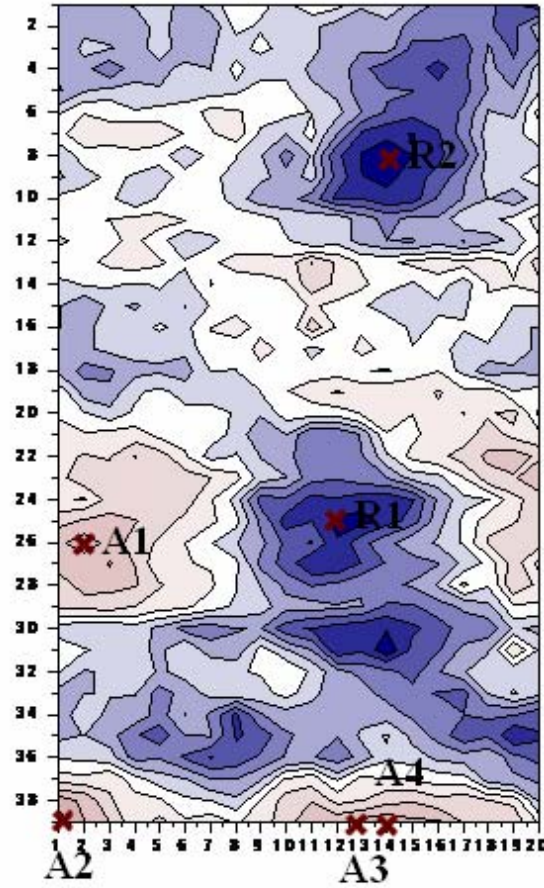**Figure 29:** NMA4; Reference point is (14, 8).

Figure 30: Frequency analysis applied to most relevant points of NMA4, with the points marked on the map. The reference point for NMA4 is R2.

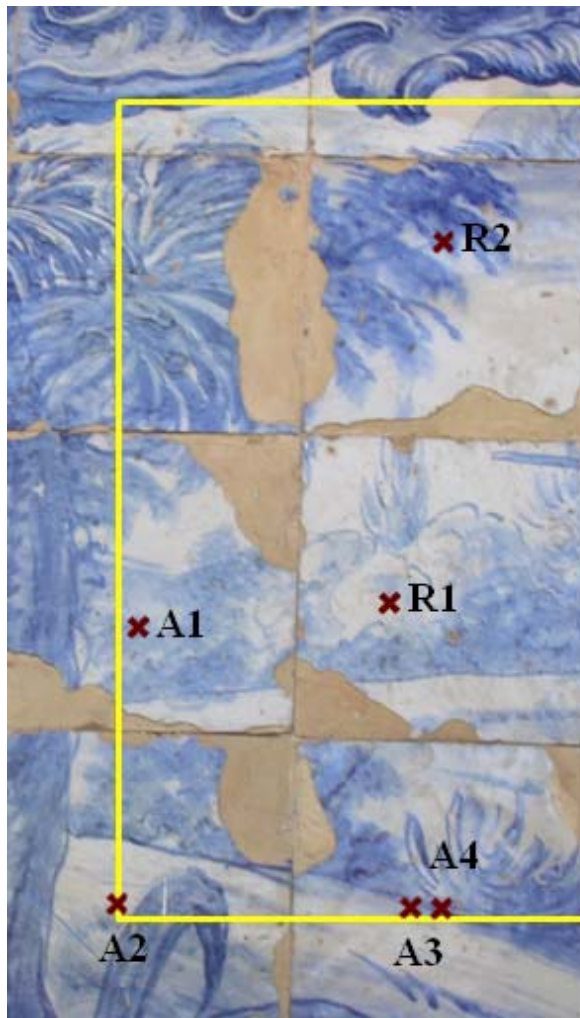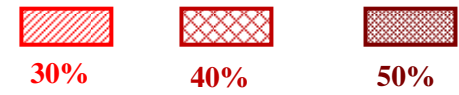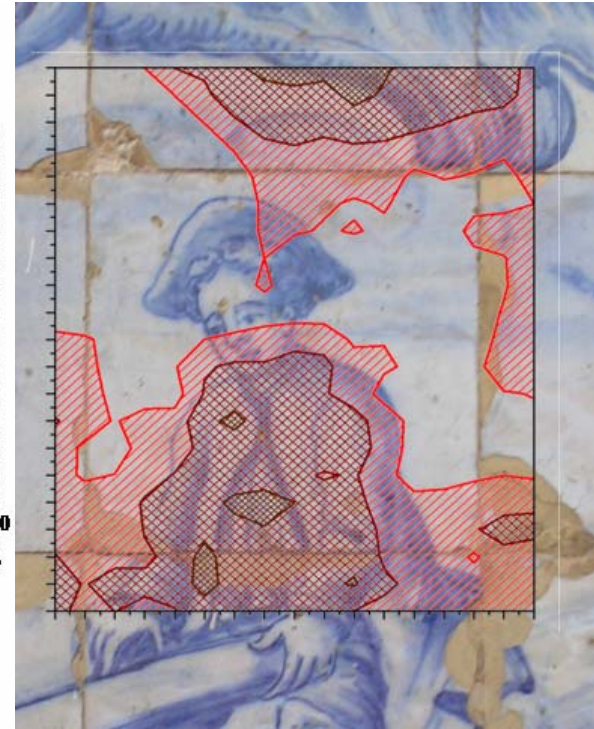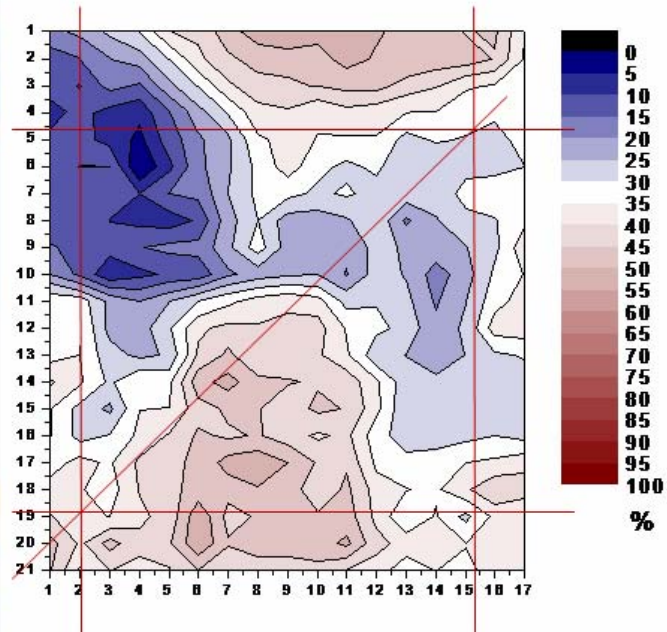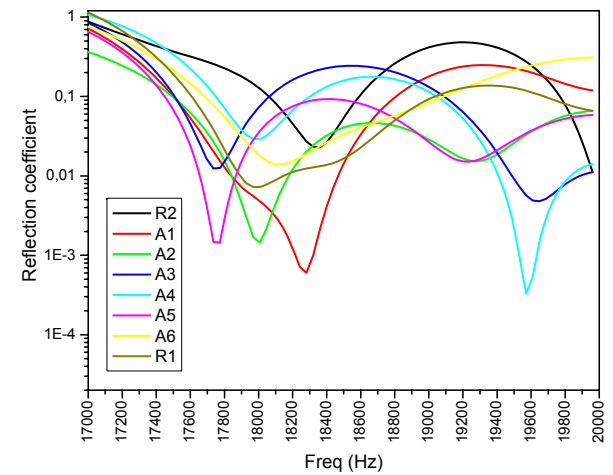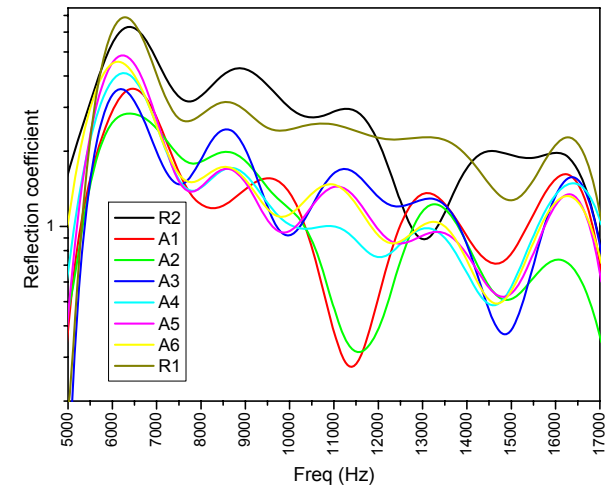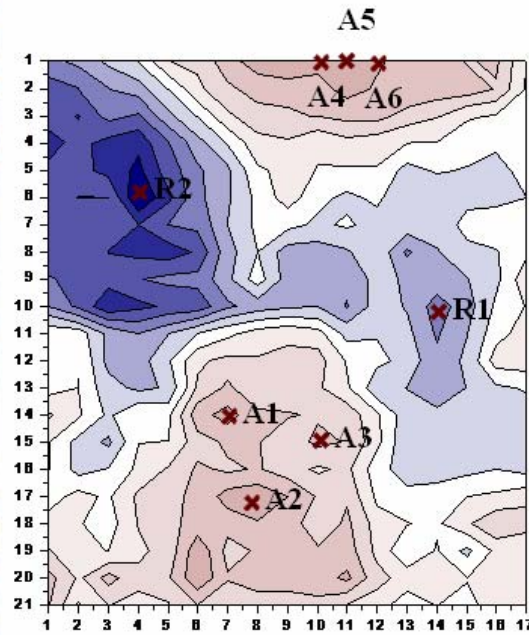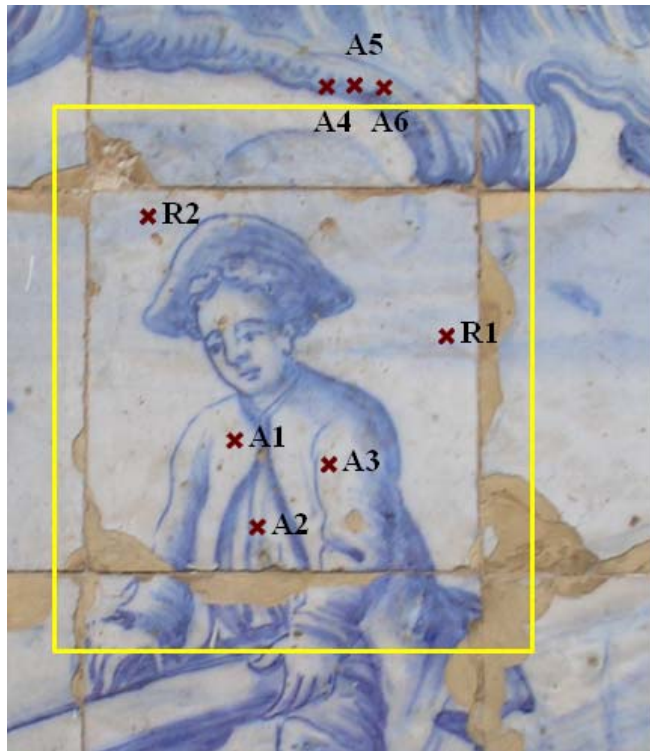**Figure 31:** NMA5; Reference point is (4, 6).

Figure 32: Frequency analysis applied to most relevant points of NMA5, with the points marked on the map. The reference point for NMA5 is R2.
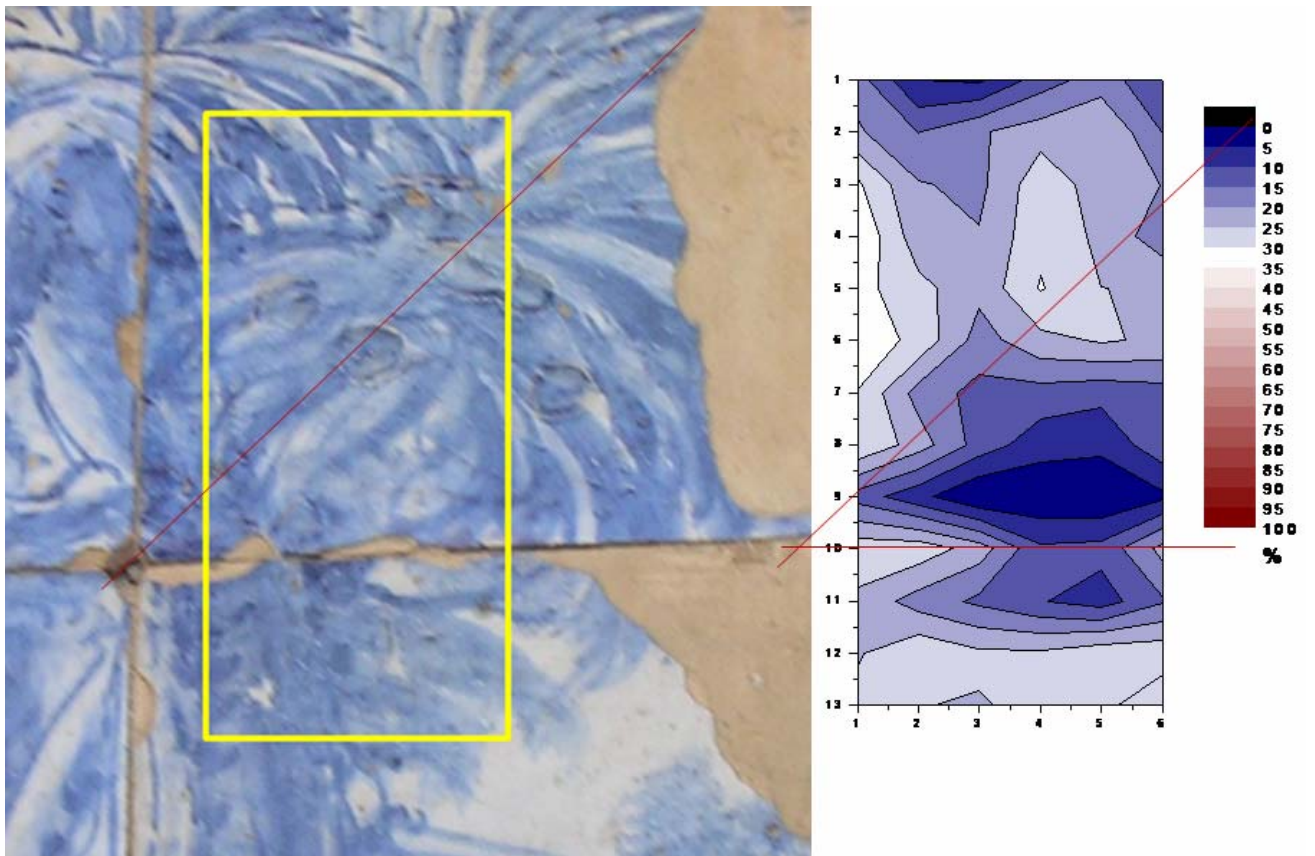
Figure 33: NMA6; Reference point is (3, 9).

10 - CONCLUSIONS

The problems of detachment and delamination in glazed ceramic tile panels have been investigated by means of *in situ* measurements based on the determination of acoustic absorption, and carried out in two locations at the Portuguese National Tile Museum. The study was directed towards the assessment of reliability of the method for tile panel diagnostics. For this purpose different approaches to data analysis have been discussed, achieving interesting indications about the usefulness of the method. Indeed the acoustic method appears to give indication about the presence of resonant cavities although the comparison with the subjective *martelletto* inspection on maps NMA1 and NMA2 does not give an apparent agreement between the results. Frequency analysis on these maps confirms the presence of few resonances in the low frequency range, below 2 kHz, and other less evident resonances in the high frequency range, between 2 kHz and 8 kHz. The high frequency resonances detected by the ACEADD method might be a possible cause of the discrepancy in the comparison of the two methods, since these frequencies are more difficult to reveal by the *martelletto* technique based on human perception.

As far as glaze delamination is concerned the acoustic method appears suitable even for the determination of thin cavities, few microns deep, since a number of resonances were clearly found in NMA4 and NMA5. But for a complete assessment of the experimental results further investigation is required about the limits of the acoustic method with respect to the minimum size of detectable defects.

Repeatability tests were realized on a restricted data set and returned important indications about the precision of the method, furthermore they were found helpful in the examination of surface heterogeneity. It has to be noted that the repeatability test performed for each map, in the specific measuring conditions, would make data analysis particularly reliable even at the first level of interpretation, which has a purely statistical approach.

Finally the resonance frequency values extrapolated from the experimental data were in good agreement with the expected range of values evaluated by the theoretical model, as described in section 4.

The experimental results give evidence to some important aspects that would improve the potential of the acoustic method. A reliable calibration procedure of the ACEADD device is strongly required, taking into account an accurate determination of the spherical spreading factor k_r, the determination of the reflection coefficient of a totally reflecting material, the validation of the signal processing algorithm with simulated data sets, and the realization of a movable sample with known absorbing characteristics constituting a reference standard for *in situ* measurements. At present an accurate calibration procedure is under study, its effect would transfer the *highly reflecting reference point* out of the

acoustic map employing a reference material as the *total reflection reference measure*. Thus an implemented measuring procedure may be applied for future works.

A further important requirement regards a systematic approach to comparison procedures with other diagnostic methods. In this work a first attempt was realized with the *martelletto* technique, but the comparison with a number of methods whose usefulness was proved for artifacts affected by similar problems may be accomplished in a more articulate cooperation between LNEC and CNR_IDASC. In particular the attention is mainly focused on glaze delamination, still representing the most difficult form of deterioration to reveal. The problems affecting the glazed layer seems to be more urgent, for the prevention of glaze loss, thus additional investigation constitute the basis for future work. Recently LNEC has successfully tried infra-red (IR) thermography on single delaminated tiles, laboratory tests exhibit promising results but the method is not yet functional for tiles adherent to walls. Once it can be usable, the acoustic method is proposed as a means to scan rapidly large panels with a view to detect problem areas. These can then be individually appraised by IR imaging with a high resolution to confirm the results and prepare a preventive intervention. On the other hand CNR_IDASC has planned some tests on tile samples, provided by LNEC, employing other acoustical methods showing high spatial resolution in order to verify their eligibility to a future comprehensive *in situ* comparison program.
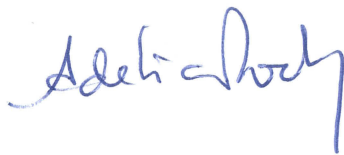
ACKNOWLEDGEMENTS

BIBLIOGRAPHICAL REFERENCES

[1] Mimoso, J-M et al. "Decay of historic azulejos in Portugal- an assessment of research needs" in Proceedings of the Int Sem *Conservation of Glazed Ceramic Tiles- research and practice*, LNEC, Lisbon April 15-16, 2009.

[2] Mimoso, J-M "Cesari Brandi's Theory of Restoration and azulejos" in Proceedings of the Int Sem *Conservation of Glazed Ceramic Tiles- research and practice*, LNEC, Lisbon April 15-16, 2009.

[3] Kinsler L. E., Frey A. R., Coppens A. B., Sanders J. V. "Fundamentals of Acoustics", John Wiley & Sons.

[4] Harris "Handbook of Acoustical Measurements and Noise Control", McGraw Hill 1991.

[5] Material database supplied by Odeon A/S (Denmark), www.odeon.dk

[6] Fahy F., "Sound and Structural Vibration. *Radiation, Transmission and Response*", Academic Press 1985.

[7] Beranek L. L., "Noise and Vibration Control", Institute of Noise Control Engineering 1989.

[8] Pereira da Silva, C. (UFPA fellowship) "Azulejos Historicos Europeus produzidos no final do seculo XIX e inicio do seculo XX: caracterização mineralógica e química de biscoitos", Revista Cientifica de UFPA.

[9] Sakagami K.., Takahashi D., Gen H., Morimoto M. "Acoustic Properties of an Infinite Elastic Plate with a Back Cavity", Acustica, vol. 78, pp. 288-295, 1993.

[10] Sakagami K.., Takahashi D., Gen H., Morimoto M. "Acoustic Properties of an Infinite Elastic Plate Backed by Multiple Layers", Acustica/Acta Acustica, vol. 82, pp. 45-53, 1996.

[11] Cox, T.J. and P. D'Antonio, Acoustic absorbers and diffusers : theory, design, and application. 2004, London ; New York: Spon Press. xxi, 405 p.

[12] G. B. Cannelli, P. Calicchia "Non-destructive acoustic method and device, for the determination of detachments of mural paintings" (European Patent EP1190243B1, 6 September 2006; US Patent US 6728661, 27 April 2004; PCT N. PCT/IT00/00244, 13 June 2000; Italian Patent N. RM 99 A000410, 25 June 1999).

[13] P. Calicchia, G. B. Cannelli "Detecting and mapping detachments in mural paintings by non-invasive acoustic techniques: measurements in antique sites in Rome and Florence", Journal of Cultural Heritage, vol. 6(2), 115-124, 2005.

[14] P. Calicchia, G. B. Cannelli "Revealing surface anomalies in structures by in situ measurement of acoustic energy absorption", Applied Acoustics, vol 63, issue 1, 43-59 (2002).

[15] J.S. Bolton, and E. Gold, 1984, The application of Cepstral techniques to the measurement of transfer functions and acoustical reflection coefficients, Journal of Sound and Vibration 93(2), 217-233.

[16] J.S. Bolton, and E. Gold, 1986, The determination of acoustic reflection coefficients by using Cepstral techniques, I: experimental procedures and measurements of polyurethane foam, Journal of Sound and Vibration 110(2), 179-202.

[17] J.S. Bolton, and E. Gold, 1986, The determination of acoustic reflection coefficients by using Cepstral techniques, II: extensions of the technique and considerations of accuracy, Journal of Sound and Vibration 110(2), 203-222.

[18] EN ISO 354:2003 "Acoustics: Measurement of sound absorption in a reverberation room".

[19] ISO 13472-1:2002 "Acoustics: Measurement of sound absorption properties of road surfaces in situ".

[20] JCGM 200:2008 "International vocabulary of metrology (VIM)".

[21] JCGM 100:2008 "Evaluation of measurement data — Guide to the expression of uncertainty in measurement (GUM 1995 with minor corrections)".

Laboratório Nacional de Engenharia Civil, Lisboa, Abril de 2010

VISTOS	**AUTORIA**

A Directora do

Departamento de Materiais

Adélia Rocha

Investigadora do LNEC

Paola Calicchia

Investigadora do

Istituto di Acustica e Sensoristica

"O. M. Corbino" (CNR_IDASC)

João Manuel Mimoso

Investigador do LNEC

INVESTIGATION ON THE PRESENCE OF DETACHMENTS IN AZULEJOS

BY MEANS OF NON DESTRUCTIVE ACOUSTIC MAPPING

ANNEXES

ANNEX 1- GLOSSARY

NOTE: bibliographical references are listed on Page 60

Absorption coefficient

Ratio of acoustic power entering the surface of the object under investigation to the incident acoustic power α=1-r, where **r** is the fraction of incident power reflected by the surface [19]. Depending on the method used to determine the absorption coefficient of an object, different definitions of α may be appropriate:

$$\alpha(\theta) = \frac{4\rho_0 c_0 \, \text{Re}(Z)\cos\theta}{\left(\text{Re}(Z)\cos\theta + \rho_0 c_0\right)^2 + \left(\text{Im}(Z)\cos\theta\right)^2} \quad \text{plane wave oblique incidence} \quad (G1)$$

$$\alpha(0) = \frac{4\rho_0 c_0 \, \text{Re}(Z)}{\left(\text{Re}(Z) + \rho_0 c_0\right)^2 + \left(\text{Im}(Z)\right)^2} \quad \text{plane wave normal incidence} \quad (G2)$$

where $\rho_0 c_0$ is the characteristic impedance of air, **Z** is the surface impedance of the object, and θ is the incidence angle.

If the reverberation room method is adopted, then the absorption coefficient is referred to the overall effect of the object on the diffuse field inside the reverberation room. It is defined as the ratio of the equivalent sound absorption area of the test specimen A_T, for which Sabine's equation is used, divided by the area of the test specimen S:

$$\alpha_S = \frac{A_T}{S} = \frac{1}{S}\left[55.3V\left(\frac{1}{c_2 T_2} - \frac{1}{c_1 T_1}\right) - 4V(m_2 - m_1)\right] \quad (G3)$$

where **V** is the volume of the reverberation room, T_2 and T_1 are the reverberation times of the reverberation room measured with and without the test specimen, m_2 and m_1 are the power attenuation coefficients, in reciprocal meters, calculated for the climatic conditions present in the reverberation room during the two measurements [19].

The absorption coefficient in diffuse field α_S is related to the oblique incidence absorption coefficient $\alpha(\theta)$ by the following equation:

$$\alpha_S = 2\int_0^{\pi/2} \alpha(\theta)\cos\theta\sin\theta d\theta . \quad (G4)$$

Bessel functions

The Bessel functions are solutions of the Bessel differential equation of order n, expressed as:

$$\left[x^2\frac{d^2}{dx^2} + x\frac{d}{dx} + \left(x^2 - n^2\right)\right]f(x) = 0 . \quad (G5)$$

Possible solutions of the equation are:

- the Bessel functions of the first kind $J_n(x)$ for all x;
- the Bessel functions of the second kind $Y_n(x)$;
- the Bessel functions of the third kind $H_n^{(1)}(x)$ and $H_n^{(2)}(x)$ for all x>0.

For $J_n(x)$ the series expansion for any generic order **n** may be given as:

$$J_n(x) = \left(\frac{x}{2}\right)^n \sum_{k=0}^{\infty} \frac{\left(-\frac{x^2}{4}\right)^k}{k!\Gamma(n+k+1)}.$$
(G6)

where **Γ(x)** is the Gamma function : $\Gamma(x) = \int_0^{+\infty} t^{x-1} e^{-t} dt$.   (G7)

The properties of the Bessel functions, approximated expressions for small or large arguments and tabulated values are found in the literature [3].

Characteristic Acoustic Impedance

The characteristic impedance of a medium is the ratio of the sound pressure at a given point to the particle velocity at that point in a free, plane and progressive wave [7]. It is a material property and equals the product of the material density (volumetric mass) ρ, expressed in kg.m^{-3}, times the speed of sound **c** in the material, expressed in m.s^{-1}:

$$Z = \rho\ c.$$
(G8)

It is expressed in Pa.s.m^{-1}.

Cepstrum Algorithm

The power <u>cepstrum</u> (pronounced "kɛpstrəm") is the inverse Fourier transform of the natural logarithm of the squared modulus of the Fourier transform of the time history of a signal [15]. Its name was derived by reversing the first four letters of "spectrum". The cepstrum can be seen as a powerful tool for separating the information carried by the excitation signal from the information carried by the response signal of the system under study.

Assuming a source S and a microphone M, mounted a certain distance L away from the source, representing the transceiver system, and assuming the pressure **p(t)** is measured at a specific distance from the reflecting surface, then:

$$p(t) = p_i(t) + p_r(t) = p_i(t) + k_r p_i(t) * h_s(t-\tau) \quad (G9)$$

where $k_r = L / (L + c\ \tau)$ is the spherical spreading factor. The acoustic pressure **p (t)** is processed by means of the Cepstrum algorithm as follows:

$$FFT[p(t)] \qquad P(\omega) = P_i(\omega) + P_r(\omega) = P_i(\omega)\left[1 + k_r H_s(\omega)e^{-i\omega\tau}\right] \qquad (G10)$$

$$Ln \qquad \ln|P(\omega)|^2 = \ln|P_i(\omega)|^2 + \ln\left[1 + k_r H_s(\omega)e^{-i\omega\tau}\right] + \ln\left[1 + k_r H_s^*(\omega)e^{i\omega\tau}\right] \qquad (G11)$$

First order approximation: $\ln[1+z] = z - {z^2}/{2} + {z^3}/{3} \dots$ for z<1 (G12)

$$IFFT\left[\ln|P(\omega)|^2\right] \qquad C(t) = C_i(t) + k_r h_s(t-\tau) + \text{higher order terms.}$$ (G13)

C(t) is the Cepstrum trace, superposition of the cepstrum of the incident wave and the impulse response corrected by the spreading factor. The function *h_s(t)* is the impulse response of the system under investigation.

Impulse Response
Output temporal signal of a dynamic system when the applied input signal is a Delta function *δ(t)*. It describes the response or the reaction of the system to some external stimulus, as a function of time. Assuming *f(t)* is the response of a system and *δ(t)* is the input signal, then the output signal is

$$\int_{-\infty}^{+\infty} f(t)\delta(t)dt = f(0); \qquad \text{and accounting for temporal shift:}$$

$$\int_{-\infty}^{+\infty} f(t)\delta(t-\tau)dt = f(\tau).$$ (G14)

Note: a Delta function is the mathematical representation of an infinitely short temporal signal carrying an energy quantity equal to unity.

Mean value
Assuming a quantity *q* that varies randomly, the arithmetic mean of the *n* independent observations *q_k* is in most cases the best available estimate of the expected value, and is written as [21]:

$$\bar{q} = \frac{1}{n}\sum_{k=1}^{n} q_k$$ (G15)

Modified Bessel function
The modified Bessel function *I_n(x)* is related to the first kind Bessel function *J_n(x)*:

$$I_n(x) = (-i)^n J_n(ix)$$ (G16)

The properties of the modified Bessel function, approximated expressions for small or large arguments and tabulated values are found in the literature [3].

Normal surface impedance
Also called Normal Specific Impedance, it is the ratio of the complex sound pressure *p(0)* to the normal component of the complex sound particle velocity *u(0)* at an individual frequency in the reference plane, where the reference plane contains the surface of the object under investigation, assumed in 0:

$$Z = \frac{p(0)}{u_\perp(0)}.$$ (G17)

It is expressed in Pa.s.m^{-1}.

Poisson's ratio

Poisson's ratio ε is the ratio of the magnitudes of the lateral strain to the longitudinal strain:

$$\varepsilon = -\frac{\varepsilon_{yy}}{\varepsilon_{xx}} = -\frac{\varepsilon_{zz}}{\varepsilon_{xx}}.$$ (G18)

The effect derives from the stretching of molecular bonds within the material lattice to accommodate the stress. The minus sign accounts for the difference in the signs of the lateral and longitudinal strains. When the applied longitudinal force is a tension and ε_{xx} is positive, then the structure of the solid induces a reduction of the lateral size and ε_{yy}, ε_{zz} are negative. Otherwise, when a compressive force is applied and the longitudinal strain is negative, then the structure of the solid induces an enhancement of the lateral size resulting in positive lateral strains. Poisson's ratio depends on the material and it usually varies between about 0.25 for glass and steel before yield and 0.5 for incompressible materials (*whose volume remains constant under compressive or tensile stress*) such as rubber [6]. Poisson's ratio of cork is close to nil because it shows very little lateral expansion when compressed.

Radius of gyration

The two-dimensional radius of gyration is used to describe the way in which the area of a cross-section is distributed around its centroidal axis. The gyration radius of a cross-sectional area **S** about the axis is useful in estimating the stiffness of a rod or plate, and is given by the following formula:

$$\kappa^2 = \frac{I}{S}$$ (G19)

where **I** is the second moment of inertia and equals the integral $\int_S y^2 dS$ where **y** is the perpendicular distance from the axis to the elemental area dS. For a rectangular section $I = bh^3/12$ with respect to its centroidal axis, where **b** and **h** are the width and height respectively, so that **I** is expressed in m^4. If the area is concentrated far from the centroidal axis it will have a greater value of κ and a greater resistance to buckling or bending. A cross-section can have more than one radius of gyration and most sections have at least two. Therefore, the section tends to buckle around the axis with the smallest value, as is the case of a section of a thin plate. The radius of gyration κ of an area about a given axis represents a distance from the axis, expressed in m.

Specific Acoustic Impedance

The specific acoustic impedance is the complex ratio of the sound pressure at a point in a medium to the particle velocity at that point. It is expressed in Pa.s.m^{-1}.

Standard Deviation

The experimental standard deviation $s(q_k)$ characterizes the dispersion of the observed values q_k, about their mean $\bar{q}$. It is defined as the square root of the variance [21]:

$$s(q_k) = \sqrt{\frac{1}{n-1} \sum_{j=1}^{n} (q_j - \bar{q})^2}$$ (G20)

Standard Deviation of the Mean

The experimental standard deviation of the mean quantifies how well the mean estimates the expectation of q and may be used as a measure of the uncertainty of $\bar{q}$, it is written as [21]:

$$s(\bar{q}) = \sqrt{\frac{s^2(q_k)}{n}} \; ; \quad \text{where} \quad u(\bar{q}) = s(\bar{q}) \quad \text{is the uncertainty of measurement} \quad$$ (G21)

Transfer Function

The Transfer Function *H(f)* is the Fourier transform of the impulse response *h(t)*:

$$H(f) = \int_{-\infty}^{+\infty} h(t) e^{2\pi i f t} \, dt$$ (G22)

Transfer Matrix Model

The Transfer Matrix Modeling of sound propagation enables the surface impedance of single and multiple layers of absorbing material to be calculated. Assuming the propagation of plane waves between the layers in the *xy* plane, and considering the continuity of pressure *p* and particle speed *u* at the boundaries, the surface pressure of one layer is related to that of the next layer [11].
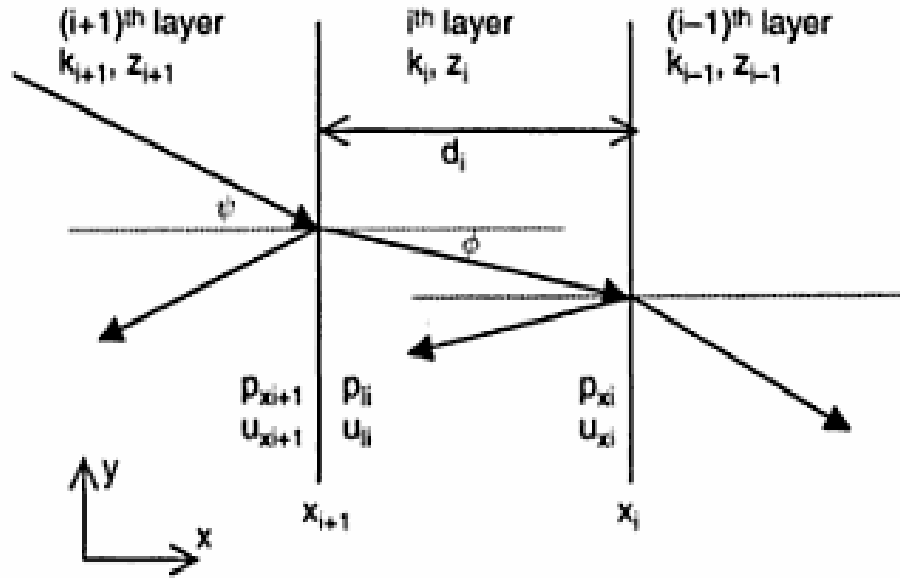
Let us assume that $\begin{Bmatrix} p_{li} \\ u_{li} \end{Bmatrix}$ represents matricially p and u at the top of the ith layer; $\begin{Bmatrix} p_{xi+1} \\ u_{xi+1} \end{Bmatrix}$ represents p and u at the bottom of the (i+1)th layer; $\begin{Bmatrix} p_{xi} \\ u_{xi} \end{Bmatrix}$ represents p and u at the bottom of the ith layer. And d_i is the ith layer thickness, ρ_i is the ith layer density, and k_{xi} is the x-direction component of the complex wave number of the ith layer, related to the incidence angle.

Then, the pressure and velocity at the top of the multilayer system is given by:

$$\begin{Bmatrix} p_{li} \\ u_{li} \end{Bmatrix} = \begin{Bmatrix} p_{xi+1} \\ u_{xi+1} \end{Bmatrix} = \begin{Bmatrix} \cos(k_{xi}d_i) & j\dfrac{\omega\rho_i}{k_{xi}}\sin(k_{xi}d_i) \\ j\dfrac{k_{xi}}{\omega\rho_i}\sin(k_{xi}d_i) & \cos(k_{xi}d_i) \end{Bmatrix} \begin{Bmatrix} p_{xi} \\ u_{xi} \end{Bmatrix} \qquad \text{(G23)}$$

from which the surface impedance of the top layer $Z_{xi+1} = p_{xi+1}/u_{xi+1}$ is calculated on the basis of the surface impedance of the bottom layer Z_{xi}. The equation is recursive and obtained simply applying boundary conditions and Snell's law for k_{xi}, the process is then repeated until each layer is evaluated.

The surface impedance of the top layer Z_{xi+1} can be written as follows:

$$Z_{xi+1} = Z_i \frac{Z_{xi} + jZ_i\dfrac{k_i}{k_{xi}}\tan(k_{xi}d_i)}{Z_i + jZ_{xi}\dfrac{k_{xi}}{k_i}\tan(k_{xi}d_i)} \qquad \text{(G24)}$$

where $\omega\rho_i$ was substituted by the equivalent form $Z_i k_i$. The ratio k_{xi}/k_i equals the cosine of the incidence angle, $\cos(\theta_i)$. For the particular case in which the system has an infinitely rigid backing wall with infinite impedance $Z_{xi} = \infty$, the surface impedance of the adjacent layer becomes:

$$Z_{xi+1} = -j\frac{Z_i}{\cos\theta_i}\cot\left(k_{xi}d_i\right).$$

(G25)

Moreover, if $\theta_i = 0$ (in the case of normal incidence) and the system is an air layer of thickness d, terminated by a rigid backing, the surface impedance reduces to:

$$Z_{aw} = -j\rho_0 c_0 \cot\left(k_0 d\right)$$

(G26)

with *ρ_0* and *c_0* the density of air and the speed of sound in air respectively.

Uncertainty of measurement

The uncertainty of a measurement is the parameter associated with the result of a measurement that characterizes the dispersion of the values that could reasonably be attributed to the measurand [21].

Young's modulus

Young's modulus *E* is defined as the ratio of longitudinal stress *σ_{xx}* to longitudinal strain *ε_{xx}* in a thin bar under longitudinal tension applied along the x axis [6]:

$$E = \frac{\sigma_{xx}}{\varepsilon_{xx}}$$

(G27)

The stress is defined as the applied force per unit area F/S, and the strain being the unitary deformation of the bar dx/x_0. It has the dimensions of [force] [length]$^{-2}$ and is expressed in Pa. In many cases in which a solid of finite size is considered, when a longitudinal tension is applied along the x axis, the sides of the solid move toward the axis producing lateral strains ε_{yy} and ε_{zz} even if no lateral constraints are present. This phenomenon is known as Poisson contraction, and the effects are expressed by means of Poisson's ratio.

ANNEX 2 – RESSONANCE FREQUENCY EVALUATION

The evaluation of resonance frequencies, for air cavities of depth d, was based on Eq. (16). The relevant quantities are:

- the sound speed in air, $c_0 = 343$ m s^{-1} at 20°C;
- the density of air, $\rho_0 = 1,292$ kg m^{-3};
- the cavity depth, d;
- the surface density of the surface layer, ρ_s.

For a cavity depth d typical values are here assumed: a) for tile detachments from the wall **d** is assumed equal to 1mm, about 10% of a characteristic tile thickness; b) for glaze delamination **d** is assumed equal to 100 μm, about 20-30% of the characteristic glaze thickness.

For surface density values a study carried out on a comprehensive set of glazed ceramic tile samples was used, where the physical, chemical and mineralogical characteristics were investigated [8]. Nineteen samples from Portugal, Germany and France were analyzed and relevant indications were provided. For the evaluation of resonance frequencies the following quantities were taken from the indications reported in the cited work:

- the volume density of the whole tile, body and glaze, ρ_{b+g} ;
- the volume density of the tile without the glaze, ρ_b;
- the thickness of the whole tile, t_{b+g};
- the thickness of the body, t_b.

From these data, the following quantities were calculated:

- the thickness of the glazed layer, $t_g = t_{b+g} - t_b$;
- the volume density of the glazed layer, $\rho_g = [\rho_{b+g} t_{b+g} - \rho_b t_b] / t_g$, assuming an equal surface S for the whole tile, for the body and the glazed layer, and a size for S of 14 cm × 14 cm which corresponds to the usual size of Portuguese tiles;
- the mass of the body, the glazed layer, and the whole tile, i.e. m_b, m_g, m_{b+g} respectively;
- the surface density of the body, the glazed layer, and the whole tile, calculated as the product of volume density ρ_i times the thickness t_i ;
- the resonance frequencies f_0, calculated by means of Eq. (16), in which the surface density calculated for the different samples and the typical value of cavity depth d are used.

Additionally, using the same equation and allowing the cavity depth to vary inside a limited range of values, from few tens per cent down to less than one per cent, the variability of f_0 was also evaluated. For this last analysis only one among the most representative samples was used; the sample P5 is close to the typical Portuguese azulejos although the whole data set confirms the great variability of physical, chemical and mineralogical properties of glazed ceramic tiles.

Density bisque	Density bisque+glaze	Thickness bisque	Thickness glaze	Thickness total	Density glaze (g/cm3)	Sample [Ref.8]	Mass bisque	Mass glaze	Mass bisque+glaze	Tile size 14cm x 14cm
ρb (g/cm3)	ρb+g (g/cm3)	tb (cm)	tg (cm)	tb+g (cm)	ρg (g/cm3)		mb (g)	mg (g)	mtot (g)	mglaze/mtot
1,93	2	0,858	0,052	0,91	3,16	P1	324,56	32,16	356,72	0,090
1,5	1,97	0,52	0,38	0,9	2,61	P2	152,88	194,63	347,51	0,560
1,56	1,73	0,61	0,285	0,895	2,09	P3	186,51	116,96	303,48	0,385
1,66	1,64	0,639	0,111	0,75	1,52	P4i	207,91	33,17	241,08	0,138
1,76	2,11	0,532	0,193	0,725	3,07	P4ii	183,52	116,31	299,83	0,388
1,58	1,75	0,97	0,03	1	7,25	P5	300,39	42,61	343,00	0,124
1,61	1,65	0,759	0,266	1,025	1,76	P6	239,51	91,97	331,49	0,277
1,61	1,66	0,811	0,039	0,85	2,70	P7	255,92	20,64	276,56	0,075
1,64	1,72	0,858	0,042	0,9	3,35	P8	275,80	27,61	303,41	0,091
1,54	1,66	0,801	0,049	0,85	3,62	P9	241,77	34,78	276,56	0,126
1,42	1,78	0,812	0,048	0,86	7,87	P10	226,00	74,04	300,04	0,247
1,87	2,2	0,655	0,025	0,68	10,85	P11	240,07	53,15	293,22	0,181
1,71	1,75	0,818	0,067	0,885	2,24	P12	274,16	29,39	303,56	0,097
1,38	1,4	0,621	0,029	0,65	1,83	P13	167,97	10,39	178,36	0,058
1,63	1,83	0,798	0,062	0,86	4,40	P14	254,95	53,52	308,46	0,174
1,59	2,15	0,878	0,022	0,9	24,50	P15	273,62	105,64	379,26	0,279
1,77	1,9	0,971	0,019	0,99	8,54	A1	336,86	31,82	368,68	0,086
1,64	1,7	1,069	0,031	1,1	3,77	A2	343,62	22,90	366,52	0,062
1,72	1,74	0,601	0,059	0,66	1,94	F1	202,61	22,48	225,09	0,100

Tile cavity depth 1E-3m; Glaze cavity depth 100,0E-6m

Surf density bisque (g/cm2)	Surf density bisque+glaze (g/cm2)	f0 (Hz)		Surf density glaze (g/cm2)	Sample	f0 (Hz)
1,66	1,82	459,95		0,16	P1	4844,45
0,78	1,77	466,01		0,99	P2	1969,11
0,95	1,55	498,67		0,60	P3	2540,09
1,06	1,23	559,49		0,17	P4i	4769,45
0,94	1,53	501,69		0,59	P4ii	2547,19
1,53	1,75	469,06		0,22	P5	4208,39
1,22	1,69	477,14		0,47	P6	2864,43
1,31	1,41	522,37		0,11	P7	6047,17
1,41	1,55	498,72		0,14	P8	5227,82
1,23	1,41	522,37		0,18	P9	4657,95
1,15	1,53	501,52		0,38	P10	3192,55
1,22	1,50	507,32		0,27	P11	3768,26
1,40	1,55	498,60		0,15	P12	5066,91
0,86	0,91	650,47		0,05	P13	8521,69
1,30	1,57	494,62		0,27	P14	3755,06
1,40	1,94	446,07		0,54	P15	2672,76
1,72	1,88	452,43		0,16	A1	4870,19
1,75	1,87	453,76		0,12	A2	5740,50
1,03	1,15	579,03		0,11	F1	5794,31

Annex 2   Resonance frequency evaluation.

The repeatability test was performed on a restricted data set of two vertical lines in maps of different surfaces, in particular L15 of map NMA2 and L11 of map NMA3. The modalities adopted are discussed in section 9.1, while the details of the four replicates are presented in the present annex. For each line two different indicators are used to represent the amount of reflected energy; the first indicator is the impulse response peak height, while the second indicator is the integral of the square impulse response over the interval of time defined by the time window, used to extract the reflection peak.

In the following pages the indicator value collected for the four replicates are reported for all points of the two lines. The first worksheet refers to line NMA2_L15 with impulse response peak height as indicator; the second worksheet refers to the same line with impulse response energy content taken as indicator. The successive worksheet refers to line NMA3_L11 with impulse response peak height as indicator; finally the last worksheet refers to the same line with impulse response energy content taken as indicator.

From the four replicates the following quantities are calculated:
- the mean value;
- the standard deviation of the four replicates;
- the standard uncertainty evaluated as the standard deviation of the mean. The relative standard uncertainty is provided too.

In the worksheets the graphs show the mean value and the relative standard uncertainty for the whole vertical line, together with the four replicates.

mean

rip0	rip1	rip2	rip3	mean	std dev	std unc	rel std unc	perc
0,474615	0,477848	0,456823	0,42664	**0,459**	**0,023**	**0,012**	0,026	2,6
0,495424	0,480472	0,451788	0,442798	**0,468**	**0,025**	**0,012**	0,026	2,6
0,531146	0,483309	0,462654	0,469723	**0,487**	**0,031**	**0,015**	0,032	3,2
0,472588	0,41411	0,454244	0,424571	**0,441**	**0,027**	**0,013**	0,030	3,0
0,556452	0,469378	0,50977	0,458036	**0,498**	**0,045**	**0,022**	0,045	4,5
0,59499	0,500004	0,536252	0,48185	**0,528**	**0,050**	**0,025**	0,047	4,7
0,564801	0,449809	0,477362	0,52368	**0,504**	**0,051**	**0,025**	0,050	5,0
0,58899	0,45118	0,490091	0,548972	**0,520**	**0,061**	**0,031**	0,059	5,9
0,651804	0,465168	0,510563	0,624973	**0,563**	**0,090**	**0,045**	0,079	7,9
0,58157	0,506615	0,429127	0,579655	**0,524**	**0,072**	**0,036**	0,069	6,9
0,560105	0,49642	0,441255	0,599888	**0,524**	**0,070**	**0,035**	0,067	6,7
0,544682	0,479831	0,456314	0,614802	**0,524**	**0,071**	**0,036**	0,068	6,8
0,572184	0,511495	0,474794	0,641542	**0,550**	**0,073**	**0,037**	0,066	6,6
0,58526	0,587227	0,520863	0,609953	**0,576**	**0,038**	**0,019**	0,033	3,3
0,576263	0,573948	0,53754	0,570074	**0,564**	**0,018**	**0,009**	0,016	1,6
0,583676	0,610944	0,546871	0,524463	**0,566**	**0,038**	**0,019**	0,034	3,4
0,588352	0,633488	0,579409	0,554464	**0,589**	**0,033**	**0,016**	0,028	2,8
0,519188	0,548666	0,525174	0,481266	**0,519**	**0,028**	**0,014**	0,027	2,7
0,5058	0,511325	0,49531	0,39715	**0,477**	**0,054**	**0,027**	0,056	5,6
0,544554	0,552218	0,541509	0,450029	**0,522**	**0,048**	**0,024**	0,046	4,6
0,529894	0,552492	0,529411	0,516436	**0,532**	**0,015**	**0,007**	0,014	1,4

Indicator: impulse response
peak
NMA2   L15

rel std unc

mean
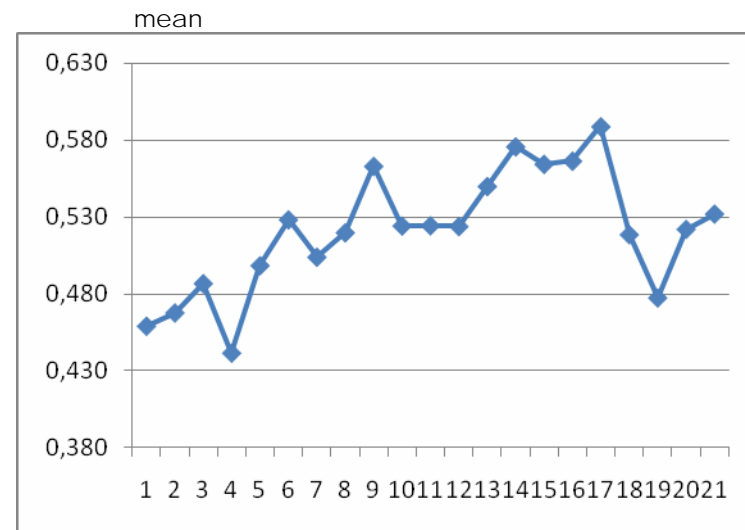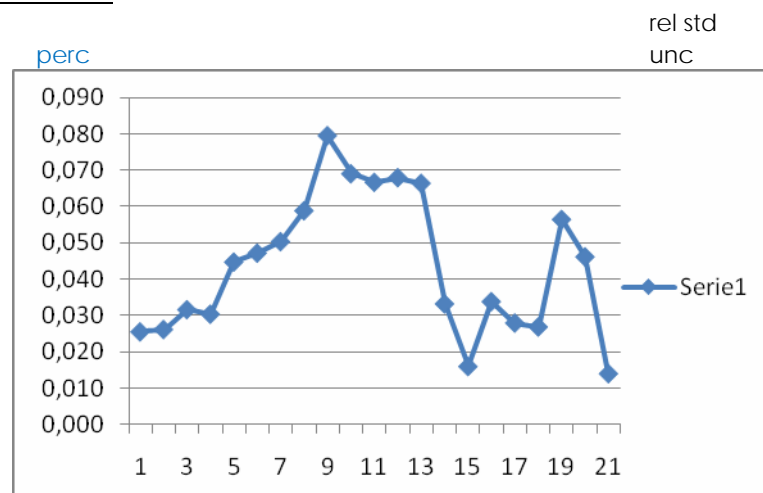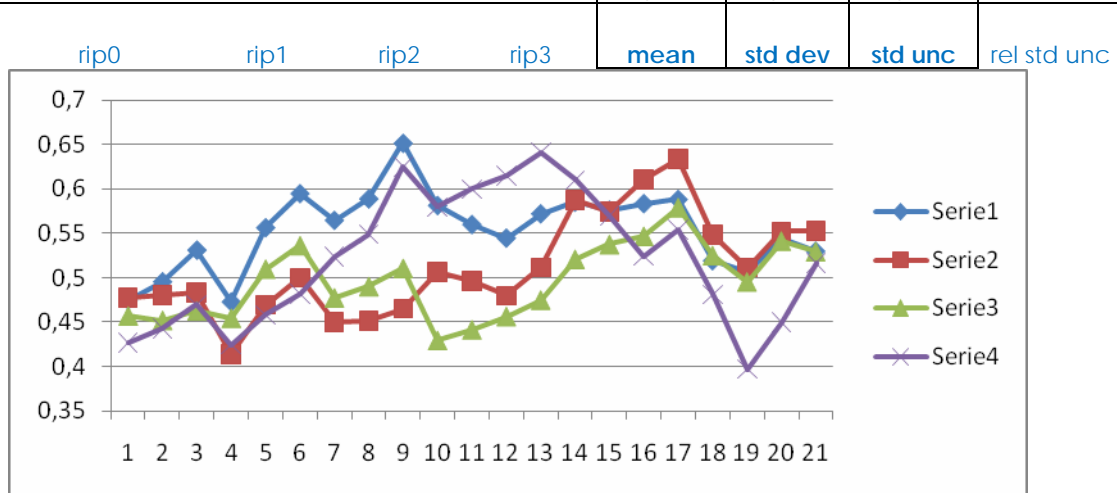
| rip0	rip1	rip2	rip3	mean	std dev	std unc	rel std unc	perc
0,101504	0,061093	0,062333	0,072758	**0,074**	**0,019**	**0,009**	0,126	12,6
0,112161	0,062696	0,064248	0,07421	**0,078**	**0,023**	**0,012**	0,148	14,8
0,129851	0,06766	0,067719	0,078714	**0,086**	**0,030**	**0,015**	0,173	17,3
0,098033	0,056025	0,056259	0,069453	**0,070**	**0,020**	**0,010**	0,141	14,1
0,1067	0,071446	0,069158	0,078926	**0,082**	**0,017**	**0,009**	0,106	10,6
0,11492	0,072861	0,072606	0,079382	**0,085**	**0,020**	**0,010**	0,119	11,9
0,108961	0,063572	0,060162	0,070208	**0,076**	**0,023**	**0,011**	0,149	14,9
0,121165	0,070631	0,068369	0,074259	**0,084**	**0,025**	**0,013**	0,150	15,0
0,132135	0,077848	0,080157	0,081735	**0,093**	**0,026**	**0,013**	0,141	14,1
0,110193	0,067396	0,08093	0,072875	**0,083**	**0,019**	**0,010**	0,115	11,5
0,102418	0,071256	0,076048	0,080127	**0,082**	**0,014**	**0,007**	0,084	8,4
0,093884	0,075478	0,082006	0,080396	**0,083**	**0,008**	**0,004**	0,047	4,7
0,113674	0,083112	0,083079	0,089664	**0,092**	**0,015**	**0,007**	0,079	7,9
0,108049	0,085711	0,087325	0,079826	**0,090**	**0,012**	**0,006**	0,068	6,8
0,096457	0,085955	0,083469	0,07575	**0,085**	**0,009**	**0,004**	0,050	5,0
0,10414	0,092839	0,082557	0,077206	**0,089**	**0,012**	**0,006**	0,067	6,7
0,106111	0,097116	0,086659	0,085348	**0,094**	**0,010**	**0,005**	0,052	5,2
0,090254	0,074089	0,071031	0,072122	**0,077**	**0,009**	**0,005**	0,059	5,9
0,086248	0,070685	0,063256	0,059066	**0,070**	**0,012**	**0,006**	0,086	8,6
0,099385	0,073894	0,072308	0,068452	**0,079**	**0,014**	**0,007**	0,090	9,0
0,098354	0,078422	0,078179	0,074373	**0,082**	**0,011**	**0,005**	0,066	6,6

Indicator: impulse response energy content

NMA2   L15

rel std unc
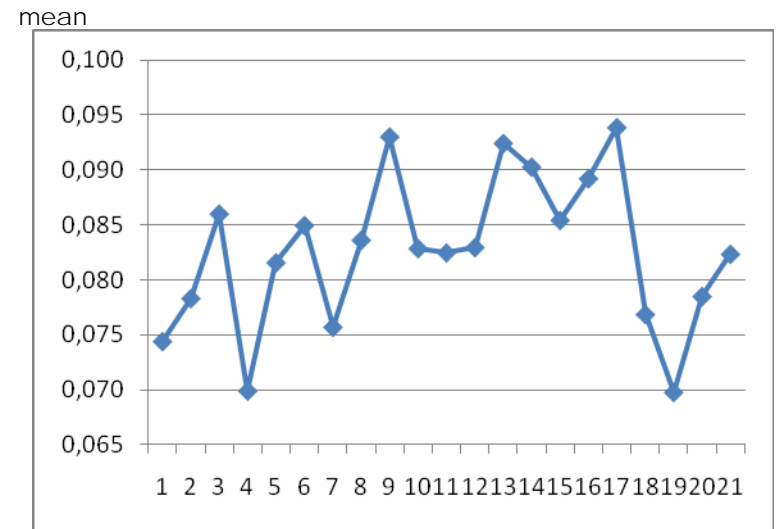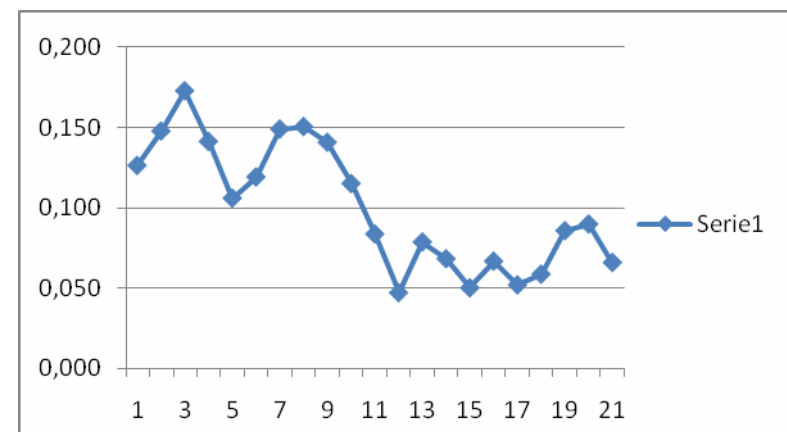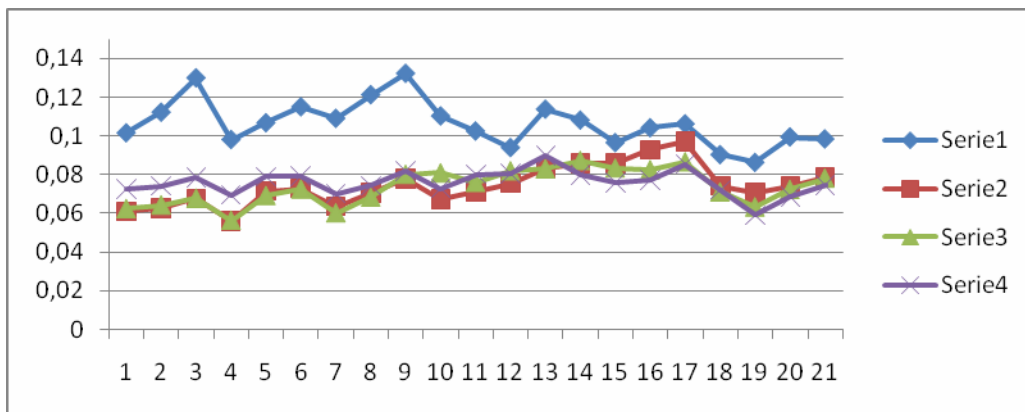
rip0	rip1	rip2	rip3	mean	std dev	std unc	rel std unc	perc
0,588949	0,543972	0,600613	0,614112	**0,587**	**0,030**	**0,015**	0,026	2,6
0,583853	0,522839	0,570881	0,607554	**0,571**	**0,036**	**0,018**	0,031	3,1
0,645041	0,629207	0,673361	0,724674	**0,668**	**0,042**	**0,021**	0,031	3,1
0,606017	0,555777	0,620468	0,646816	**0,607**	**0,038**	**0,019**	0,032	3,2
0,614594	0,524318	0,631572	0,644891	**0,604**	**0,054**	**0,027**	0,045	4,5
0,580901	0,495822	0,595959	0,610891	**0,571**	**0,052**	**0,026**	0,045	4,5
0,600772	0,540454	0,633143	0,656396	**0,608**	**0,050**	**0,025**	0,041	4,1
0,556246	0,51703	0,588511	0,587482	**0,562**	**0,034**	**0,017**	0,030	3,0
0,54097	0,518473	0,545883	0,568789	**0,544**	**0,021**	**0,010**	0,019	1,9
0,553627	0,560611	0,584128	0,605426	**0,576**	**0,024**	**0,012**	0,020	2,0
0,575554	0,543403	0,594728	0,660816	**0,594**	**0,050**	**0,025**	0,042	4,2
0,584785	0,54659	0,612518	0,640482	**0,596**	**0,040**	**0,020**	0,034	3,4
0,58411	0,557584	0,625808	0,628703	**0,599**	**0,034**	**0,017**	0,029	2,9
0,562335	0,490629	0,607453	0,591619	**0,563**	**0,052**	**0,026**	0,046	4,6
0,621714	0,523932	0,61423	0,615234	**0,594**	**0,047**	**0,023**	0,039	3,9
0,59357	0,546498	0,599694	0,610794	**0,588**	**0,028**	**0,014**	0,024	2,4
rip0	rip1	rip2	rip3	**mean**	**std dev**	**std unc**	rel std unc	perc

mean
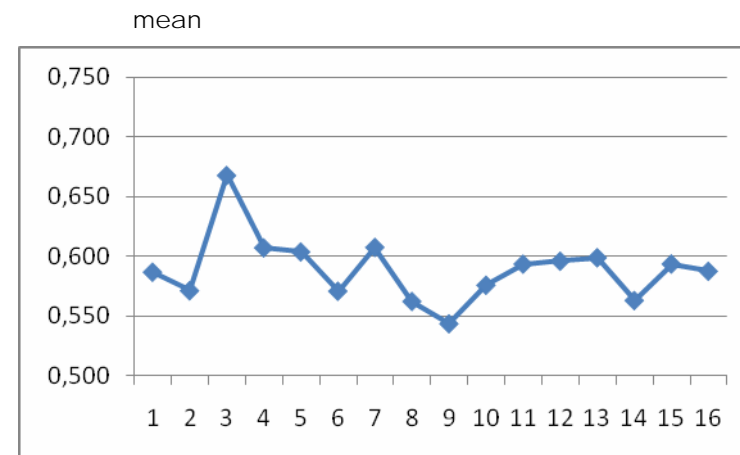
Indicator: impulse response
peak
NMA3   L11

rel std unc
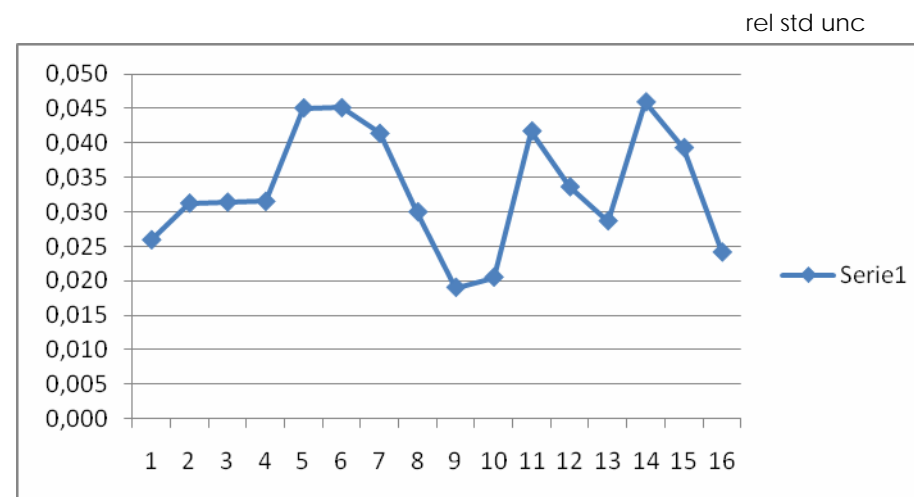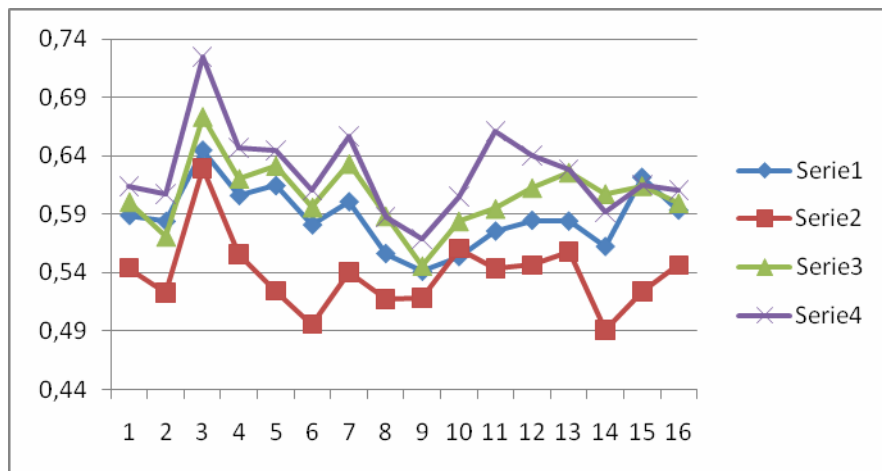
Annex 3   Repeatability test.

rip0	rip1	rip2	rip3	mean	std dev	std unc	rel std unc	perc
0,071484	0,075189	0,090674	0,098643	**0,084**	**0,013**	**0,006**	0,076	7,6
0,073331	0,072	0,081406	0,091807	**0,080**	**0,009**	**0,005**	0,057	5,7
0,089562	0,097645	0,104402	0,125896	**0,104**	**0,016**	**0,008**	0,075	7,5
0,082758	0,088277	0,085216	0,10293	**0,090**	**0,009**	**0,005**	0,050	5,0
0,084839	0,084663	0,08805	0,0988	**0,089**	**0,007**	**0,003**	0,037	3,7
0,075419	0,075881	0,075246	0,086408	**0,078**	**0,005**	**0,003**	0,035	3,5
0,075157	0,082768	0,087099	0,103358	**0,087**	**0,012**	**0,006**	0,068	6,8
0,069989	0,080974	0,082949	0,094581	**0,082**	**0,010**	**0,005**	0,061	6,1
0,065756	0,072628	0,076683	0,091733	**0,077**	**0,011**	**0,005**	0,072	7,2
0,070149	0,081913	0,092895	0,101253	**0,087**	**0,014**	**0,007**	0,078	7,8
0,068402	0,081074	0,092159	0,100716	**0,086**	**0,014**	**0,007**	0,082	8,2
0,07175	0,084155	0,092706	0,102546	**0,088**	**0,013**	**0,007**	0,074	7,4
0,072847	0,084497	0,093273	0,103637	**0,089**	**0,013**	**0,007**	0,074	7,4
0,073105	0,071784	0,079284	0,08727	**0,078**	**0,007**	**0,004**	0,045	4,5
0,092873	0,075288	0,088974	0,09772	**0,089**	**0,010**	**0,005**	0,054	5,4
0,08177	0,078175	0,079057	0,092922	**0,083**	**0,007**	**0,003**	0,041	4,1

mean

Indicator: impulse response Energy content
NMA3   L11

rel std unc